Targeting CDK4 overcomes EMT-mediated tumor heterogeneity and therapeutic resistance in KRAS mutant lung cancer

Aparna Padhye
The University of Texas MD Anderson Cancer Center
Jessica Konen
The University of Texas MD Anderson Cancer Center
B. Leticia Rodriguez
The University of Texas MD Anderson Cancer Center
Jared Fradette
The University of Texas MD Anderson Cancer Center https://orcid.org/0000-0001-6712-2860
Joshua Ochieng
The University of Texas MD Anderson Cancer Center
Lixia Diao
The University of Texas MD Anderson Cancer Center https://orcid.org/0000-0001-6995-4492
Jing Wang
UT M.D. Anderson Cancer Center https://orcid.org/0000-0002-5398-0802
Wei Lu
The University of Texas MD Anderson Cancer Center
Luisa Solis
The University of Texas MD Anderson Cancer Center https://orcid.org/0000-0002-1253-630X
Harsh Batra
The University of Texas MD Anderson Cancer Center
Maria Gabriela Raso
The University of Texas MD Anderson Cancer Center https://orcid.org/0000-0003-2105-5556
Michael Peoples
Translational Research to Advance Therapeutics and Innovation in Oncology (TRACTION), The University of Texas MD Anderson Cancer Center, Houston, TX
Rosalba Minelli
Translational Research to Advance Therapeutics and Innovation in Oncology (TRACTION), The University of Texas MD Anderson Cancer Center, Houston, TX
Alessandro Carugo
University of Texas MD Anderson Cancer Center https://orcid.org/0000-0001-5182-3320
Christopher Bristoe

Translational Research to Advance Therapeutics and Innovation in Oncology (TRACTION), The University of Texas MD Anderson Cancer Center, Houston, TX

Don Gibbons (dlgibbon@mdanderson.org)

The University of Texas MD Anderson Cancer Center https://orcid.org/0000-0003-2362-3094

Article

Keywords: lung cancer, therapeutic resistance, intratumor heterogeneity

Posted Date: April 1st, 2021

DOI: https://doi.org/10.21203/rs.3.rs-355354/v1

Targeting CDK4 overcomes EMT-mediated tumor heterogeneity and therapeutic resistance in KRAS mutant lung cancer

Aparna Padhye[1,2], Jessica M. Konen[1], B. Leticia Rodriguez[1], Jared J. Fradette[1], Joshua K. Ochieng[1], Lixia Diao[3], Jing Wang[3], Wei Lu[4], Luisa S. Solis[4], Harsh Batra[4], Maria G. Raso[4], Michael D. Peoples[5], Rosalba Minelli[5], Alessandro Carugo[5], Christopher A. Bristow[5], Don L. Gibbons[1,6*]

1. Department of Thoracic/Head and Neck Medical Oncology, University of Texas MD Anderson Cancer Center, Houston, TX 77030, USA.
2. University of Texas Graduate School of Biomedical Sciences, Houston, TX 77030, USA.
3. Department of Bioinformatics and Computational Biology, University of Texas MD Anderson Cancer Center, Houston, TX 77030, USA.
4. Department of Translational Molecular Pathology, University of Texas MD Anderson Cancer Center, Houston, TX 77030, USA
5. TRACTION Platform, Division of Therapeutics Development, University of Texas MD Anderson Cancer Center, Houston, TX 77030, USA.
6. Department of Molecular and Cellular Oncology, University of Texas MD Anderson Cancer Center, Houston, TX 77030, USA.

*Corresponding author. Email: dlgibbon@mdanderson.org

Conflict of interest statement

D.L.G. declares advisory board work for Janssen, AstraZeneca and Sanofi. D.L.G. has received research grant funding from AstraZeneca, Janssen, Astellas, Ribon Therapeutics, NGM Therapeutics and Takeda. All other authors declare that they have no conflict of interests.

Abstract

Lack of sustained response to therapeutic agents in patients with K-Ras mutant lung cancer poses a major challenge and arises partly due to intratumor heterogeneity that defines phenotypically distinct tumor subpopulations. To attain better therapeutic outcomes it is important to understand the differential therapeutic sensitivities of tumor cell subsets. Epithelial-to-mesenchymal transition (EMT) is a biologic phenomenon that can alter the phenotypic state and cause transcriptional rewiring to produce distinct tumor cell populations. We utilized functional shRNA screens, *in vitro* and *in vivo* models to identify and confirm an increased dependence of mesenchymal tumor cells on CDK4 for survival, as well as a mechanism of resistance to MEK inhibitors. High ZEB1 levels in mesenchymal tumor cells repressed p21, leading to perturbed CDK4 pathway activity. Increased dependence on CDK4 rendered mesenchymal cancer cells particularly vulnerable to selective CDK4 inhibitors. Co-administration of CDK4 and MEK inhibitors in heterogeneous tumors effectively targeted different tumor subpopulations, subverting the resistance to either single agent treatment.

Introduction

Activating *KRAS* mutation is one of the most frequent oncogenic events in lung cancer, occurring in about 30% of lung adenocarcinoma patients[1-3]. Despite the identification of the oncogene over 20 years ago and efforts to effectively treat this subset of patients, 5-year survival rates remain dismal[4]. Unlike *EGFR* mutant lung cancer, K-Ras oncoproteins are largely undruggable, with the very recent exception of the $KRAS^{G12C}$ allele[5,6]. Pharmacological inhibitors of the MAPK pathway (e.g., MEK), such as selumetinib and trametinib are available, but preclinical and clinical trials have demonstrated poor responses to MEK inhibitors[7]. Combination of MEK inhibitors with conventional chemotherapy did not demonstrate any added benefit to progression free survival[8]. Resistance to MEK inhibitors may be intrinsic (*de novo*) due to tumor cell heterogeneity or acquired due to tumor evolution as an adaptive response to pharmacological agents. In either case, the presence of phenotypically distinct tumor cell subpopulations with reprogrammed cellular machinery makes it difficult to effectively eliminate the broader tumor cell population. To address this, we need to understand the differences in the tumor cell subpopulations within a heterogeneous tumor.

Genetically identical tumor cells possess the ability to undergo transcriptional reprogramming to activate alternate survival pathways and evade therapeutic targeting. Research from our group and others has extensively demonstrated that epithelial-to-mesenchymal transition (EMT) is a central phenomenon occurring in K-Ras mutant lung cancer. A subset of cancer cells undergoing EMT contribute to intracellular tumor heterogeneity, increased metastatic potential, therapeutic resistance to pharmacological agents and poor patient outcomes[9-11]. A previously described murine lung cancer models driven by *Kras* and *p53* mutations recapitulated EMT-mediated tumor cell heterogeneity with the ZEB1/miR-200 double negative feedback loop playing a central role in dynamically altering the cellular phenotype[10]. Cancer cell lines derived from this model were classified into two groups: metastasis-incompetent, epithelial-like phenotype

with low ZEB1, high miR-200 and metastasis-competent, mesenchymal-like phenotype with high ZEB1, low miR-200. This model is capable of recapitulating cellular phenotypes within the spectrum of EMT. Our previous research highlighted the reliance of K-ras mutant epithelial lung cancer cells on activated MAPK signaling pathway and increased susceptibility to MEK inhibitors. On the other hand, tumors demonstrating a mesenchymal phenotype remained largely unresponsive to MEK inhibitors. Moreover, after an initial response to MEK inhibition, epithelial tumors acquired therapeutic resistance by undergoing EMT[11,12]. The study identified an unmet need to develop therapeutic approaches to target distinct tumor subpopulations within heterogeneous K-ras mutant lung tumor to achieve a robust therapeutic response. Utilizing multiple loss-of-function shRNA screens, we analyzed the transcriptome of the phenotypically different tumor subpopulations and identified CDK4-RB as a major survival pathway in mesenchymal tumor cells. We validated our finding using multiple *in vitro*, *ex vivo* and *in vivo* models well suited for studying EMT-mediated tumor cell heterogeneity.

CDK4 acts as a master integrator of mitogenic signaling cascades by initiating the inactivation of the central tumor suppressor RB and cell cycle commitment at the restriction point allowing cells to transition to S phase[13]. The CDK4 axis is altered in many cancers, with clinically approved pharmacologic inhibitors showing promising antitumor activity[14]. Breast cancers are frequently treated with CDK4 inhibitors in combination with hormone therapy to achieve significant tumor suppression. Some studies have shown that CDK4 and cyclin D1 expression is correlated with the presence of *KRAS* mutation in lung tumors[15] and a synthetic lethal interaction occurs between K-ras^{G12V} and CDK4 in lung cancer tumor progression[16,17]. We found that the differential activation of the CDK4 pathway in epithelial and mesenchymal cancer cells was determined by ZEB1-mediated transcriptional regulation of p21. As an intrinsic regulator of CDK4, p21 levels in cells determine the downstream CDK4 pathway activity. Our study demonstrates in multiple preclinical models that intrinsic and acquired MEK inhibitor resistance is associated with a rewired

kinome in tumors by which the mesenchymal phenotype activates the CDK4 pathway as a common occurrence across models. This CDK4 signaling dependence resulted in a potential therapeutic approach to combine MEK and CDK4 inhibitors to target different tumor subpopulations for a more robust tumor response and combat resistant outgrowth of epigenetic subsets in a heterogeneous tumor.

Results

Mesenchymal lung cancer cells exhibit increased dependency on CDK4 for growth

In order to effectively target the mesenchymal tumor subpopulations within heterogeneous tumors, we sought to identify the survival dependencies of these tumor cells. A loss of function screen with a barcoded, pooled small hairpin RNA (shRNA) library targeting about 500 genes with known kinase activity (Kinome) was conducted. Each gene was targeted with 10 unique shRNA sequences to limit false hits due to off-target effects. This library of shRNAs was transduced into representative non-metastatic, epithelial (393P) and metastatic, mesenchymal (344P) murine lung cancer cell lines derived from a previously described KP genetically engineered mouse model (GEMM) [10]. The cell lines stably expressing the shRNAs from the Kinome library were either cultured *in vitro* or implanted subcutaneously in nude mice (Fig. 1A). Tumors were harvested, shRNA barcodes were quantified by deep sequencing and referenced with the respective *in vitro* cell population and quality control measures were completed to ensure sufficient barcode coverage across the library was maintained *in vivo* (supplementary Fig. S1A, supplementary Table S1). The phenotypic impact of gene knockdown was inferred by the redundant shRNA activity (RSA) algorithm, where a lower rank of the shRNA barcodes signified dropout from the population and greater dependency on the gene for tumorigenesis (supplementary Table S2). Although both cell line models have activating $Kras^{G12D}$ and $p53^{R172H}$ mutations, comparison of the results of the Kinome screen revealed that the mesenchymal cell line (344P) and the matched syngeneic tumors were more reliant on *Cdk4* for *in vitro* and *in vivo* growth (Fig. 1B). Other top hits identified in the screen as more significant in mesenchymal than epithelial cells were *Aurka, Atr, Pik3Ca, Plk1, and Adrbk2* (Fig. 1B), consistent with recent publications about the role of the spindle assembly checkpoint in mesenchymal cells[18]. We also compared these results to our previously published FDAome shRNA[11] screen performed in a similar manner and identified *Cdk4* as the most consistent hit across *in vitro* and *in vivo* conditions

in both screens (Fig.1B, supplementary S1A, supplementary Table S3, and supplementary Table S4). CDK4 mRNA expression in a panel of 118 human NSCLC cell lines showed a positive correlation with our previously reported 76-gene EMT signature[19] (Fig. 1C) and higher expression in murine mesenchymal lung cancer cells (supplementary Fig. S1B). TCGA dataset analysis of lung adenocarcinoma patients revealed alterations in the CDK4-RB core pathway in about 30-40% of the cases (supplementary Fig. S1C), which represents over 40,000 new patients annually. These analyses demonstrate the importance of CDK4 pathway in patients with lung adenocarcinoma.

To functionally validate the shRNA screen and determine whether response to CDK4 inhibitors is dependent on the EMT status of tumor cells, we treated a panel of human and murine KRAS mutant NSCLC cell lines, stratified as either epithelial or mesenchymal based on previous profiling[10,19], with CDK4 inhibitors. Both human and murine mesenchymal NSCLC cells were more sensitive to the CDK4 inhibitors palbociclib, abemaciclib and ribociclib (Fig. 1D, Table 1). Alteration of EMT status by manipulation of the ZEB1/miR-200 axis can induce an epithelial or mesenchymal shift in tumor cells. We therefore utilized isogenic pairs of human (H441) and murine (393P) epithelial cell lines with ZEB1 expression to produce a mesenchymal phenotype[20] and isogenic pairs of human (H1299) and murine (344SQ) mesenchymal cells with miR-200 expression to push the cells to an epithelial state[21]. Comparisons across the different cell line pairs revealed that sensitivity to all CDK4 inhibitors was determined by the EMT status (supplementary Fig. S1D, S1E and Table 1).

RB and FoxM1 are important readouts for CDK4 kinase activity, whereas phospho-CDK4 may continue to be present for another 24 hours post inhibitor treatment. Suppression of the RB and FoxM1 was observed in mesenchymal cells upon treatment with abemaciclib and ribociclib for 24 and 48 hours (Fig. 1E). Epithelial tumor cells showed an initial suppression of CDK4 targets, but it was not a sustained response. The mesenchymal 344SQ cells showed a more robust

response to the inhibitor palbociclib over a range of concentrations and at shorter treatment times compared to epithelial cells (393P) in terms of suppression of downstream signaling and induction of apoptosis (supplementary Fig. S1F). In addition to pharmacologic inhibition, we also employed a genetic approach to confirm the dependency of mesenchymal tumor cells on CDK4 for survival. Mesenchymal cell lines with an inducible shRNA targeting CDK4 showed a greater reduction in tumor cell growth (Fig. 1F), with suppression of phospho-RB (Fig. 1G) compared to epithelial cells. In fact, epithelial 393P tumor cells appeared to have slightly greater growth rate with CDK4 knockdown than the control cells (Fig. 1F) and continued RB phosphorylation.

The CDK4 pathway is dynamically regulated by the EMT status of tumor cells

Because the primary role of CDK4 is cell cycle regulation at the G1-S transition, we next tested if there are phenotypic differences in the manner which epithelial and mesenchymal NSCLC cell lines undergo cell cycle progression. Upon serum starvation for 48 hours, epithelial 393P cells almost completely (~90% of the cells) arrested in the G0-G1 phase of the cell cycle with a complete suppression of the CDK4 pathway (Fig. 2A, B). In contrast, the mesenchymal cells resisted cell cycle arrest in serum free conditions, with ~80% of the cells in G0-G1 state but 20% of cells continuing to cycle through S or G2/M (Fig. 2A). This observation corresponded to higher levels of CDK4, Cyclin D1 and phospho-RB in the cells when assayed by subcellular fractionation (Fig. 2B), suggesting that CDK4 activity in mesenchymal tumor cells could be uncoupled from extrinsic mitogenic signals. After release of cells from the arrested state by addition of serum containing media, the mesenchymal cells transitioned into S phase more readily (within 20 hours) than the epithelial cells, which remained arrested in G1 phase up to 36 hours before returning to the baseline cycling state (Fig. 2A). Although cell cycle arrest in G1 phase with palbociclib was essentially similar between 393P and 344SQ cells, a significant increase in the percentage of 344SQ cells in G0 state (apoptotic cells) was detected (supplementary Fig. S2A, B), corresponding to increased cleaved caspase-3 (supplementary Fig. S1F).

Using reverse phase protein arrays (RPPA), we screened a panel of previously characterized isogenic murine epithelial and mesenchymal lung cancer cell lines and observed an increase in CDK4 axis related molecules, phospho-RB and Cyclin D1 (as downstream markers for CDK4 signaling pathway activation), in cells with a mesenchymal phenotype (supplementary Fig. S2C). A subcellular fractionation assay also showed higher levels of phospho-RB, Cyclin D1 and CDK4 in mesenchymal cells (supplementary Fig. S2D). Immunofluroscent staining of tumor cells also demonstrated an activated CDK4/RB axis with a higher percentage of 344SQ tumor cells with positive nuclear staining for phospho-CDK4 and phospho-RB and a stronger staining for total CDK4 (Fig. 2C).

We next tested the effects of altering the EMT status of tumor cells on the CDK4 signaling pathway using the previously described isogenic cell line pairs. ZEB1 overexpression in murine (393P) and human (H441) epithelial cells produced higher levels of CDK4 and phospho-RB (Fig. 2D, 2E). Conversely, miR-200 expression in murine (344SQ) and human (H1299) cells caused a suppression of the CDK4 axis (Fig. 2D, 2E). Additionally, stable ZEB1 knockdown rendered the mesenchymal KP 344SQ cells less sensitive to palbociclib (supplementary Fig. 2SE). Immunohistochemistry on mesenchymal 344SQ syngeneic tumors revealed higher phospho-CDK4 and phospho-RB staining with absent phospho-Erk, and the reverse was observed in the epithelial 393P syngeneic tumors (Fig. 2F).

We have previously observed that epithelial 393P tumors initially respond to MEK inhibitors (e.g. AZD6244), however, long-term exposure leads to acquired resistance with the acquisition of a mesenchymal phenotype (393P-AZD^{R}) [11]. We investigated whether tumors that have acquired resistance to MEK inhibitors have an activated CDK4 pathway. 393P-AZD^{R} tumors showed higher phospho-CDK4 and phospho-RB staining, with suppressed phospho-Erk, an observation similar to the *de novo* 344SQ mesenchymal tumors (Fig. 2F). Cell lines derived from 393P-AZD^{R} tumors showed higher phospho-CDK4 and ZEB1 expression, with generally lower

levels of phospho-Erk (Fig. 2G). Resistant cells were no longer sensitive to AZD6244, and instead became sensitive to palbociclib with an IC50 similar to 344SQ cells (Fig. 2H), and greater suppression of phospho-RB and phospho-CDK4 in 393P-AZD^R than in 393P-vehicle cell lines. In contrast, there was an accumulation of phospho-CDK4 in 393P-vehicle cells (supplementary Fig. S2F). We conclude that tumor cells with a mesenchymal-like phenotype, either due to intrinsic factors or arising from epithelial cells undergoing EMT as an adaptive resistance mechanism, have rewired survival pathways that activate CDK4 signaling.

ZEB1 regulates p21 expression and causes differential CDK4 pathway activation

To identify the mechanistic basis of the differential dependency on the CDK4 pathway between the phenotypic epithelial and mesenchymal cancer cells, we investigated the intrinsic regulators of CDK4 activity, p21 (*WAF1/CIP1*) and p27 (*KIP1*). Transient knockdown of p21 had a more significant impact on the phosphorylation of CDK4 and RB compared to p27 (Fig. 3A and supplementary S3A). The much higher phospho-RB in 393P cells indicated that p21 maintains a check on the CDK4-RB pathway in the epithelial cells and when disrupted causes increased activation of the pathway. Loss of p21 in mesenchymal cells only modestly increased phospho-RB compared to the control cells, suggesting that an intrinsic deficiency of p21 protein in the mesenchymal cells could lead to a dysregulated CDK4 pathway. Immunofluorescence assay on 393P, 393P-AZD^R and 344SQ cells revealed that a higher percentage of epithelial cells had nuclear p21 than mesenchymal cells, along with higher co-localization of CDK4 and p21 in epithelial tumor cells (Fig. 3B). Since alterations in the tumor suppressor *TP53* is one of the most commonly occurring co-mutation events in KRAS driven lung cancer and because p21 is a direct target of p53, we wanted to determine the effect of p53 and whether any differences might account for CDK4 pathway regulation in the epithelial and mesenchymal tumor cells. With transient knockdown of p53, we did not observe any significant difference in downstream pathway signaling (supplementary Fig. S3B, S3C). Additionally, we also utilized previously published *Kras^{G12D}*

mutant (K1) and *Kras*^{G12D}*/p21*$^{-/-}$ (KC3 and KC4) murine tumor cells[22] to determine if p21 could regulate the sensitivity of tumor cells to CDK4 inhibitors. Absence of p21 in tumor cells sensitized KC cell lines to palbociclib with an increase in CDK4 signaling (supplementary Fig. S3D, S3E). This further emphasized that p21-mediated CDK4 dysregulation was independent of p53 control.

Our previously published microarray datasets[10] that interrogated differential gene expressions demonstrated that epithelial-like cancer cells have a higher expression of *Cdkn1a* (gene encoding for p21), including comparisons of 344SQ vs 393P cells (fold change 0.57, $p=0.003$) and 393P-ZEB1 vs 393P-vector (fold change 0.27, $p<0.0001$). We confirmed and extended this observation with a panel of murine cell lines and found that p21 mRNA levels inversely correlated with ZEB1 mRNA levels across the panel (Fig. 3C, supplementary S3F). Analysis of *CDKN1A* mRNA expression in 29 KRAS mutant human lung adenocarcinoma cell lines revealed an inverse correlation with a previously published EMT gene signature[19] (Fig. 3D). Immunohistochemistry analysis of epithelial (393P) and mesenchymal (344SQ) and 393P-AZD^{R} tumors also showed an inverse correlation between p21 and ZEB1 levels (Fig. 3E). Pathologic analysis of human NSCLC samples for ZEB1 and p21 by IHC staining revealed an inverse correlation between nuclear ZEB1 and p21 H-scores (Fig. 3F). We also grouped the samples based on low ZEB1 (<4 H-Score) or high ZEB1 (>4 H-score) staining and found a significant difference in p21 H-score (supplementary Fig. S3G). Combined together the data support the regulation of p21 by EMT status and more specifically by ZEB1.

We further tested this observation by inducing EMT or MET by overexpression of ZEB1 or miR-200 in human and murine isogenic cell line pairs. We observed p21 transcriptional and translational repression with ZEB1 expression. Conversely, with miR-200 expression, there was an upregulation of p21 (Fig. 3G, 3H). Transient and stable knockdown of ZEB1 in human and murine cells, respectively, caused p21 expression (supplementary Fig. S3H, S3I and S3J). Cells treated with the HDAC inhibitor mocetinostat undergo an MET by upregulation of the miR-200

family and ZEB1 suppression[11,23]. Treatment also produced increased expression of p21 (supplementary Fig. S3K, S3L and S3M). Induction of miR-200 in tumor cells by different means pushes the cells to a more epithelial state, which is generally considered a less aggressive phenotype for tumor cells and more akin to a "normal" cell state. Expression of p21 in an epithelial like state restores the cell cycle checkpoint that is lost or blunted in mesenchymal tumor cells with high ZEB1 activity and a more aggressive phenotype.

Luciferase reporter assays were utilized to investigate ZEB1 mediated transcriptional regulation of p21. The promoter region of p21 was cloned upstream of a luciferase reporter and transfected into human lung cancer cells with either ZEB1 or miR-200 expression. H358 and H441 cells expressing ZEB1 led to a decrease in relative luciferin signal confirming transcriptional repression of the p21 promoter in the presence of high ZEB1. Conversely, an increase in luciferin signal was detected in H1299 cells with miR-200 induction, which suppresses the endogenous cellular ZEB1 expression and relieves transcriptional repression of the p21 promoter (Fig. 3I). Binding of ZEB1 to the endogenous p21 promoter was confirmed by ChIP qPCR assays in cells with inducible ZEB1 or miR-200 expression, using previously published primer pairs[24] (Fig. 3J). Using GAPDH as the negative control and miR-200c as a positive control, we confirmed direct binding of ZEB1 to the p21 promoter.

Suppression of p21 in mesenchymal cells regulates CDK4 pathway

We next explored the effect of p21 on CDK4 activity in epithelial and mesenchymal lung cancer cells. With transient knockdown of CDK4 (supplementary Fig. S4A), phosphorylation of RB was continuously suppressed in mesenchymal cells for 48 hours (Fig. 4A). On the contrary, CDK4 knockdown in epithelial tumor cells appeared to have only slightly muted downstream signaling (phosphorylation of RB), which coincided with a rather surprising accumulation of phosphorylated CDK4, even with very low levels of total CDK4 protein (Fig. 4A). The CDK4

accumulation corresponded to a continued presence of p21 protein in the epithelial cells (Fig. 4A). The intriguing findings observed here recapitulated the data in a previous report by Bisteau et al.[25], which showed that a sustained presence of p21 protein in cells was able to maintain the phosphorylation status of CDK4 (and hence the stability of the complex), but still inhibit its kinase activity. A similar observation was made in our epithelial model, but not mesenchymal, where the presence of p21 maintains the CDK4 in the phosphorylated state. To further demonstrate this point, we co-immunoprecipitated CDK4 and p21 in mesenchymal and epithelial cancer cells (Fig. 4B). In mesenchymal 344SQ and 344SQ_vector cells, lower amounts of CDK4-p21 complex co-immunoprecipitated together compared to epithelial 393P and 344SQ_miR-200 cells where an increased binding of CDK4 and p21 was detected. We also observed the seemingly contradictory presence of phospho-RB in epithelial cells alongside p21 expression (Fig. 4A). An explanation for this observation is the sequestration of p21 into the CDK4 complex, alleviating the repression from the CDK2-Cyclin E complex, which can then phosphorylate RB to maintain cell cycle progression. In fact, we observed that epithelial cells are more sensitive to the CDK2 inhibitor (miciclib) than mesenchymal cells (supplementary Fig. S4B), indicating that CDK2 may be the primary regulator of cell cycle in epithelial cells. A similar outcome was observed with pharmacological inhibition of CDK4 (supplementary Fig. S4C), including a partial suppression of phospho-RB, an accumulation of phospho-CDK4 with the presence of p21 in epithelial cells, versus a lack of p21 with a near complete suppression of phospho-RB in the mesenchymal cells by 48 hours. Lower binding of p21 to CDK4 in mesenchymal cancer cells is only sufficient to maintain the activity of the CDK4 complex but not in abundant enough to exert an inhibitory effect on the downstream pathway.

Constitutive (344SQ_pCMV6) or doxycycline-induced (344SQ_pTripZ) expression of p21 in the mesenchymal 344SQ cells was used to determine the direct effect of p21 on CDK4 activity. Upon p21 expression, there was suppression of phospho-RB and phospho-CDK4, which

correlated with detection of higher amounts of the CDK4-p21 complex (Fig. 4C, 4F). These cells also demonstrated slower *in vitro* growth compared to the vector only cells (Fig. 4D, 4G) and a decreased sensitivity to palbociclib (supplementary Fig. S4D, S4F). When the cells were implanted subcutaneously in syngeneic wildtype mice, the p21 overexpressing tumors grew significantly slower (Fig. 4E, 4H and supplementary Fig. 4SE, 4SG), with about one-third of tumors undergoing complete regression. We also generated 393P cells with stable or doxycycline-inducible knockdown of p21 (supplementary Fig. S4H, S4L). A modest increase in phospho-RB was detected with p21 knockdown (supplementary Fig. S4I, S4M), along with slightly higher growth rates (supplementary Fig. S4J, S4N) and enhanced sensitivity of the epithelial 393P cells to palbociclib (supplementary Fig. S4K, S4O).

Since we observed that CDK4 levels are critically linked with the EMT status of cells, we wanted to exploit this observation for therapeutic purposes. With doxycycline-mediated induction of CDK4 shRNA, we observed an MET and decreased ZEB1 levels and an accumulation of phospho-Erk (Fig. 4I), which indicated that targeting CDK4 shifts the tumor population to a more epithelial state, that would prime the tumor cells for MEK inhibitor treatment. To test this hypothesis, we transiently knocked down CDK4 in mesenchymal cells and treated with AZD6244, which sensitized the previously unresponsive mesenchymal 344SQ and 344P cells to MEK inhibition (Fig. 4J). We also tested the effect of combination palbociclib and AZD6244 treatment, using a series of fixed concentrations and calculated the fraction affected (Fa) values after exposure to the drugs. The Chou-Talalay method[26] was used to determine the combination index (CI) and drug reduction index (DRI). The favorable DRI, shown in yellow (Fig. 4K), was used to confirm the CI data. The drug combinations showed favorable DRI (DRI>1) and evidence of synergism (CI<1) at Fa>0.5 for palbociclib and AZD6244 (Fig. 4K). Additionally, when tumor cells were treated with single-agent MEK or CDK4 inhibitor, there was a reciprocal activation of the CDK4 or MEK signaling pathways, respectively (Fig. 4L), showing a dynamic switching of

316 signaling pathway activation and survival dependencies in the face of pharmacological
317 treatments.

318 **Co-targeting CDK4 and MAPK pathways targets different tumor cell subsets**

319 We have previously described that MEK inhibitors preferentially target epithelial K-ras
320 mutant tumor cells[11,12] and with the evidence presented here that CDK4 inhibitors have a greater
321 impact on mesenchymal tumor cells, we set out to test the effects of combination treatment on
322 the tumor cell subpopulations. To test if the pharmacological inhibitors have differential apoptotic
323 effects on tumor subpopulations, we treated human (H1299 and H358) and murine (393P and
324 344SQ) tumor cells with AZD6244 and palbociclib and stained the cells with annexin V and
325 propidium iodide. Both human (H1299) and murine (344SQ) mesenchymal tumor cells underwent
326 greater apoptosis in response to CDK4 inhibitors and epithelial tumor cells (H358 and 393P) were
327 highly sensitive to MEK inhibition (Fig. 5A, 5B and supplementary Fig. S5A, S5B).

328 Given that tumors are heterogeneous and consist of cell subsets with distinct phenotypes,
329 we utilized a previously described sensor model, which can detect the epithelial or mesenchymal
330 state of individual tumor cells in real time[12,27]. Briefly, the 344SQ_Z-cad cell line expresses dual
331 fluorescent sensors: a destabilized GFP with the ZEB1 3' UTR cloned downstream and E-
332 cadherin promoter driving expression of RFP. This tool exploits the ZEB1/miR-200 double
333 negative feedback loop, which tightly regulates EMT. In an epithelial state, with high miR-200 and
334 E-cadherin, the cells express RFP and emit red fluorescence and the presence of miR-200
335 suppresses GFP production by binding to the ZEB1 3'UTR and preventing translation.
336 Conversely, in a mesenchymal state with high ZEB1 and low miR-200, cells emit green
337 fluorescence on account of GFP translation, whereas ZEB1 binds to the E-cadherin promoter to
338 suppress transcription of RFP. As seen in Fig. 5C, the majority of the cells in 2D culture were
339 mesenchymal and GFP^+. With treatment of mocetinostat, there was an enrichment of RFP^+

epithelial cells. We utilized this system to test if CDK4 and MEK inhibitors differentially target epithelial and mesenchymal subpopulations. We observed a reduction of epithelial RFP cells with MEK inhibitor (AZD6244) treatment and mesenchymal GFP cells with CDK4 inhibitor (palbociclib) treatment (Fig. 5C, 5D). With dose escalation of single agent treatment, reciprocal pathway activation occurred, while combination treatment with both drugs suppressed MAPK and CDK4 pathways (supplementary Fig. S5D) and enhanced tumor cell killing. Since western blots are bulk assays, we wanted to assess which specific populations undergo apoptosis within this heterogeneous dynamic system. We utilized a DNA binding dye that is cleaved by caspases present in the cells undergoing apoptosis to produce blue fluorescence, which can be detected by microscopy and flow cytometry. Co-localization of blue/green fluorescence with palbociclib treatment and blue/red fluorescence with AZD6244 treatment demonstrated the specificity of each individual drug to target specific cell types, whereas the combination of both drugs targeted both subpopulations (Fig. 5E, supplementary Fig. S5E).

In vitro three dimensional assays very closely recapitulate the tumor growth *in vivo*. An established *ex vivo* tumor (EVT) model to culture lung tumors that retains tumor cell heterogeneity[28] was utilized to test the therapeutic sensitivity of distinct tumor cell subpopulations (Fig. 5F). Similar to the observations in 2D cultures, we found different subpopulations being targeted by individual drugs when EVTs were cultured in laminin-rich Matrigel (MG). Since MG is known to promote an epithelial phenotype[10,28,29], MEK inhibition effectively eliminated this cell subtype and resulted in an enrichment of the GFP^+ cells. The CDK4 inhibitor, conversely, caused a depletion of mesenchymal tumor cells within the heterogeneous EVTs and enrichment of the RFP^+ cells. We also noted a change in phenotype of EVTs treated with palbociclib, producing more structures with a central lumen as compared to other groups (supplementary Fig. S5F). Lumen formation and organization in a 3D matrix is characteristic of epithelial cells. Clearly, treatment with CDK4 inhibitor not only targets mesenchymal cells but also promotes an epithelial

phenotype, which makes it ideal to be combined with MEK inhibition. In combination treatment, both populations were targeted, which produced a net decrease in size and viability of EVTs (Fig. 5F and supplementary Fig. S5G). EVTs were also cultured in a matrix containing MG and collagen I, and as previously noted collagen promotes a mesenchymal phenotype in tumor cells[21,28], which made it ideal to test the efficacy of CDK4 inhibitor on this specific subpopulation. MEK inhibitor remained ineffective on the GFP^+ mesenchymal tumor cells, however, there was a significant reduction in the viability of EVTs with CDK4 treatment (Fig. 5G). Combination treatment proved to be significantly better over the individual treatments in both Matrigel and collagen matrices in terms of suppression of viability of tumor cells. In summary, these results demonstrate the efficacy of CDK4 and MEK inhibitors in combination for effective therapeutic targeting of the lung cancer subpopulations.

Combination of CDK4 and MEK inhibitors controls syngeneic tumor growth and prevents emergence of EMT-mediated resistance

We next evaluated *in vivo* tumor response to the combination of CDK4 and MEK inhibitors. Mesenchymal (344SQ) or epithelial (393P) tumor cells were subcutaneously implanted in syngeneic wildtype mice. Tumor growth in response to either single agent (palbociclib or AZD6244) or combination was monitored over a period of 6-14 weeks. Mice bearing 344SQ tumors remained unresponsive to AZD6244, but responded to palbociclib alone or in combination with AZD6244 (Fig. 6A). The short treatment for ~6 weeks scored as additive using Bliss effect analysis[30] (supplementary Fig. S6A). This promising tumor response in the short term led us to repeat the experiment to determine if there was a durable and sustained response to the combination treatment. Treatment of the cohorts for up to 10 weeks produced the emergence of resistance to palbociclib treatment alone (Fig. 6B). The tumors acquired resistance to single agent palbociclib over an extended period of time, which was prevented with combination treatment, and the group initially treated with only palbociclib was resensitized upon addition of AZD6244 at

week 10, either as measured by tumor growth or fold change of tumor volume (Fig. 6B/C). We also observed an increase in E-cadherin and a decrease in nuclear ZEB1 with single-agent palbociclib treatment (Fig. 6D), demonstrating the selection for an epithelial phenotype. The combination treatment for a period of 14 weeks scored as an additive response (supplementary Fig. S6A). The number of lung metastatic nodules in short- and long-term experiments were also significantly lower with palbociclib or combination treatment (supplementary Fig. S6B, S6D, S6E).

Epithelial tumors that initially respond to AZD644 will develop resistance to treatment by undergoing EMT. When treated with single agents, 393P tumors were resistant to palbociclib alone and responded to AZD6244 for about 7 weeks (Fig. 6E). However, the combination of both the drugs suppressed tumor growth with a durable response for ~10 weeks. In the 393P tumor model, combination of CDK4 and MEK inhibitor scored as synergistic using the Bliss effect analysis (supplementary Fig. S6A). Since 393P is a non-metastatic model, there were no significant differences in lung metastases (supplementary Fig. S6C, S6F). Previously described 393P-vehicle and 393P-AZD^{R} cells were also implanted subcutaneously in syngeneic wildtype mice to assess the sensitivity to CDK4 and MEK inhibitors. 393P-vehicle tumors retained their sensitivity to AZD6244 and resistance to palbociclib (supplementary Fig. S6G), whereas the tumors derived from 393P-AZD^{R} cells were unresponsive to AZD6244, and responsive to palbociclib, with one mouse showing complete tumor regression (Fig. 6F and supplementary Fig. S6H).

Primary tumor tissues were collected at the end of the mouse experiments and stained for the CDK4 and MAPK signaling pathway markers. Untreated 344SQ tumors showed higher phospho-CDK4 and phospho-RB compared to untreated 393P tumors, which had higher phospho-Erk (Fig. 6G). In 344SQ tumors, treatment with palbociclib led to suppression of phospho-CDK4 and phospho-RB staining, with an activation of MAPK signaling as marked by phospho-Erk; AZD6244 treatment lead to an increase in phospho-CDK4, and the combination

drug treatment suppressed both CDK4 and MAPK signaling. 393P tumors, on the other hand, showed suppression of phospho-Erk when treated with AZD6244, accompanied with an increased expression of phospho-Cdk4. Palbociclib caused an increase in phospho-Erk in 393P tumors as well. Combination drug treatment in both models suppressed both pathways significantly compared to either single agent (Fig. 6G).

To determine the effect of single and combination agent treatments on cell proliferation and cell death, we performed Ki67 staining and TUNEL assay on the tumor tissues. 344SQ tumors treated with palbociclib for 6 weeks had fewer proliferating and more apoptotic cells (Fig. 6H, 6I). 393P tumors treated with AZD6244 had fewer proliferating cells and higher apoptotic cells (Fig. 6H, 6J). However, combination inhibitor treatment in both models significantly suppressed cell proliferation and produced apoptosis in >60% of the tumor cells. We also compared the cell proliferation and death in the 344SQ tumors treated long term (10 weeks) with the single agents and combination. As noted, the 344SQ tumors acquired resistance to palbociclib alone after 10 weeks. This was reflected in the Ki67 and TUNEL staining, which were similar to 344SQ tumors treated with AZD6244, which were unresponsive (supplementary Fig. S6I, S6J). With co-administration of AZD6244 after 10 weeks of single agent palbociclib, tumors underwent apoptosis with limited cell proliferation, similar to the tumors treated with combination from the start of the experiment (supplementary Fig. S6I, S6J). Tumor growth and histological staining collectively demonstrate the efficacy of utilizing a combinatorial approach for treatment of heterogeneous tumors with different tumor subpopulations.

Concomitant targeting of CDK4 and MAPK pathways augments response in Kras mutant autochthonous lung tumors

Autochthonous lung tumor models represent powerful and accurate preclinical models for recapitulating human cancer and exploration of treatment efficacy. Three different Kras mutant

GEM models were utilized to interrogate the CDK4 pathway in lung tumors, as well as response to palbociclib alone or in combination with AZD6244. Lung tumors in these models harbor either Kras point mutation G12D (*Kras*$^{LSL/+}$ (Kras)) alone or coupled with homozygous deletion of p53 (*Kras*$^{LSL/+}$*; P*$^{flox/flox}$ (KP)) or homozygous deletion of miR-141/200c (*Kras*$^{LSL/+}$*; M*$^{-/-}$ (KM)) [11,31]. Schematic representations of the different alterations are presented in supplementary Fig. S7A. These conditional autochthonous lung tumors were generated through intratracheal administration of adenovirus expressing Cre recombinase[31]. Histological analyses on lung tumors displayed differences in signaling pathways across the different genetic backgrounds (Fig.7A). Tumors with mutant Kras alone showed greater MAPK pathway activation compared to KP and KM tumors, which instead showed an activation of CDK4 pathway as demonstrated by phospho-CDK4 and phospho-RB staining (Fig. 7A). We also utilized these models to interrogate if the ZEB1-p21 axis was altered within these tumors and could determine their sensitivity to palbociclib. Tumor regions with high nuclear ZEB1 corresponded to lower levels of nuclear p21 in KP and KM tumors as compared to Kras tumors alone (Fig. 7B).

Three months after induction, lung tumor formation was confirmed and monitored over 6-8 weeks by micro-CT scans for changes in overall lung tumor burden in response to pharmacological agents. Response to AZD6244 alone across all three genotypes was similar to our previous[11] results where K-ras tumors showed complete regression upon treatment and only partial response was achieved in KP and KM tumors (supplementary Fig. 7C, S7B, S7C). Palbociclib alone had more significant tumor growth control in KP and KM mice than AZD6244 alone with ~30% of tumors undergoing complete regression (Fig. 7B, supplementary Fig. S7B, S7C). Histological staining showed that treatment with each single agent led to an activation of reciprocal signaling pathway in KP and KM tumors (Fig. 7D, 7E). Palbociclib led to suppression of ZEB1 indicating a shift to an epithelial phenotype and AZD6244 led to an accumulation of ZEB1 indicating the presence of mesenchymal tumor cells (Fig. 7D, 7E). Combination of palbociclib and

AZD6244 produced a more significant reduction of tumors over a period of 8 weeks with complete regression in ~80% mice across the three genotypes (Fig. 7C, supplementary Fig. S7B, S7D). Lack of sufficient tumor burden precluded us from staining the lung sections obtained from combination treatments.

Fig. 7F shows the working model for the activation of the different survival pathways in the phenotypically distinct epithelial and mesenchymal tumor cells. Normal cells or epithelial cancer cells have an intact cell cycle regulation mediated by the intrinsic regulator p21. Increased binding of p21 to CDK4 prevents the kinase activity, limits RB phosphorylation and arrests cells in the G1 phase. However, this pathway is dysregulated in cancer cells undergoing EMT. ZEB1 is highly upregulated in mesenchymal cancer cells, which exerts transcriptional repression on p21. Lack of p21 leads to low or no binding of p21 to CDK4, allowing the kinase activity of CDK4 to occur unchecked. Such high dependency on CDK4 makes mesenchymal cells especially vulnerable to CDK4 inhibitors such as palbociclib. In heterogeneous tumors, with epithelial and mesenchymal cancer cells, net tumor killing requires drug combinations that preferentially target the vulnerabilities of each subpopulation (e.g., MEKi and CDK4i).

Discussion

Phenotypic switching and subsequent transcriptional rewiring in cancer cells in response to the tumor microenvironment or selective pressures of drug treatments allows the escape of cancer cells from cell death. An understanding of the mechanisms by which tumor cells alter their cellular state and molecular pathways can provide the basis for designing effective therapeutic strategies. Epithelial to mesenchymal transition is a dynamic phenomenon that contributes to tumor heterogeneity in cancer. We demonstrate that lung tumors with high ZEB1 that display mesenchymal phenotype have increased dependence on the CDK4 pathway for survival, which renders them especially vulnerable to CDK4-specific pharmacological inhibitors. Combined with

488 the results previously published from our lab that showed higher sensitivity of epithelial cancer
489 cells to MEK inhibitors[11], we investigated the combination of CDK4 and MEK inhibitors in multiple
490 *in vitro* and *in vivo* models that recapitulate EMT-mediated tumor heterogeneity and demonstrated
491 that the combination of CDK4 and MEK inhibition in Kras mutant lung adenocarcinoma is an
492 effective strategy to combat EMT-mediated heterogeneity and therapeutic resistance.

493 CDK4 plays a key role in determining the progression of cells from G1 to S phase of the
494 cell cycle. Disruption of the checkpoint leads to unregulated growth in cancer cells. Ordinarily, the
495 cell cycle is regulated by extracellular mitogenic signals that are integrated by the MAPK
496 pathway[14,32]. However, aberrant CDK4 activation in Kras mutant mesenchymal cancer cells can
497 occur in a cell autonomous manner, without being coupled with extrinsic signals or the MAPK
498 pathway. Thus, the independent activation of CDK4 serves as a survival mechanism activated in
499 mesenchymal cancer cells allowing escape from MEK inhibitors. Interestingly, epithelial tumor
500 cells are less dependent on CDK4 for survival, as shown by the stable knockdown of CDK4 and
501 insensitivity to pharmacological inhibitors. Instead, CDK2-dependent RB phosphorylation seems
502 to be the major cell cycle pathway in epithelial cancer cells. A previous study identified that MAPK
503 mediated activation of CDK2 keeps a check on RB activity and prevents progression of Kras
504 mutant lung cancers[33]. This is in line with our observations in the epithelial cancer cells that have
505 activated MAPK pathway and a proper cell cycle regulation. Although the results from Walter et
506 al.[33] were not studied in the context of EMT, our results show that the epithelial tumor cells are
507 equally receptive to CDK2 and MEK inhibitors, whereas mesenchymal cancer cells are resistant.
508 These findings reiterate the fact that CDK4 and MAPK pathways are closely linked in lung cancer
509 and present an opportunity for therapeutic co-targeting.

510 Separate studies have presented contradictory findings for the correlation of EMT with
511 CDK4 pathway signaling. CDK4 inhibition in triple negative breast cancer reversed the EMT status
512 of cancer cells[34,35], as seen in the 344SQ mesenchymal tumors treated with palbociclib in the

present study. Within Kras-mutant pancreatic cancer, one study showed that tumor cells underwent EMT with palbociclib monotherapy[36] and MET in another[37]. Another study in colorectal cancer noted no difference in EMT status of tumor cells in response to palbociclib[38]. These findings highlight the fact that there are cell-type or context-specific phenomena that warrant further investigation in different cancer types. In our studies, we found that modulation of the EMT status of cancer cells by perturbing the ZEB1/miR-200 axis lead to CDK4 pathway modulation and determined the sensitivity to CDK4 inhibitors both *in vitro* and *in vivo*.

Mechanistically, we identified that high ZEB1 in mesenchymal cancer cells was responsible for transcriptional repression of *CDKN1A* (gene encoding for p21) by direct binding to the promoter region. Conventionally, p21 is described as a suppressor of CDK4 kinase activity and a downregulation/loss in patients predicts poor survival[39,40]. Studies in the recent years have further explored the role of p21 and revealed a dual function of p21, acting in some cases as an activator for CDK4 activity[41]. Lower levels of p21 binding are generally required for the assembly and stability of the CDK4-cyclin D complex. p21 binding to CDK4 partially accounts for maintaining phosphorylation of CDK4, primes CDK4 for catalysis by releasing the activation segment without affecting kinase function (e.g. phosphorylation of RB) [25]. On the other hand, a sustained presence of p21 at higher stoichiometric concentrations can render CDK4 ineffective[25]. We found that mesenchymal cancer cells had lower levels of p21 in the CDK4-p21 complex, which explains increased CDK4 activity. Continued presence of an activated CDK4 rendered the mesenchymal cells highly dependent on CDK4 for survival. Increased addiction to CDK4 translated to *de novo* vulnerability to CDK4 inhibitors. With p21 overexpression in mesenchymal cancer cells, we detected increased CDK4-p21 complex, reduced *in vitro* and *in vivo* growth of tumors. Interestingly, 344SQ cells demonstrated reduced sensitivity to palbociclib with p21 overexpression. A previous study had shown that p21 can interfere with the binding of small inhibitors to CDK4 complex, as we observe in wild type epithelial tumor cells and in p21

overexpressing mesenchymal cells[42]. Thus, p21 serves as a regulator of CDK4 activity and sensitivity to inhibitors in mesenchymal lung cancer cells.

ZEB1 mediated p21 regulation was demonstrated by utilizing isogenic pairs of cell lines expressing ZEB1 or miR-200 as well as by treatment by mocetinostat, an HDAC inhibitor. Mocetinostat induces miR-200 expression, which can relieve ZEB1 repression on the p21 promoter. Mocetinostat can also regulate the HDACs that are present in co-repressor complexes with ZEB1[23]. Evidence from past studies suggested that class I HDACs (HDAC1, 2 and 3) repress the p21 promoter as part of NuRD, Sin3A, NCoR-SMRT co-repressor complexes[43]. Recent work from our lab demonstrated that ZEB1 is present in such co-repressor complexes to regulate promoter activity of important genes altered in cancer progression[44]. There is also evidence that a trimeric complex of ZEB1, HDAC1/2 and p53 in stromal fibroblasts promotes breast cancer progression[45]. Independently, p53 is a well-established regulator of p21 expression which occurs in response to oncogenic stress to induce cell cycle arrest and/or apoptosis[46,47]. Loss of p53 in cancer can lead to the downregulation of p21 and unchecked cell growth[47], however we did not observe a direct effect of p53 on p21 expression to regulate the CDK4 pathway. Evidently, a complex network of transcriptional regulators determine p21 levels in the cells and further investigations are warranted to understand these intricacies. Our findings do highlight that correlation of EMT status and p21 levels can serve a biomarker for response to CDK4 inhibitors in lung cancer patients.

With an understanding of how lung cancer cells adapt to therapeutic intervention, we interrogated the combination of CDK4 and MEK inhibitors. Normal cells possess intact cell cycle checkpoints and are spared by selective CDK4 inhibitors. CDK4 inhibition causes tumor cell senescence or apoptosis in addition to cell cycle arrest making these cancer cells particularly vulnerable to the inhibitors[48]. The remarkable success of CDK4 inhibitors in combination with endocrine therapy in breast cancer patients have encouraged investigations into the role of CDK4

563 inhibitors in other cancer types, including lung cancer[49-52]. K-Ras^{G12V} driven lung cancers were
564 particularly susceptible to ablation of CDK4 with an induction of senescence and prevention of
565 tumor progression[17]. A sustained tumor response was also achieved with concomitant CDK4
566 inactivation and RAF1 ablation in *Kras/p53* driven lung cancers[16]. A phase II trial in NSCLC
567 patients with inactivated *CDKN2A* treated with palbociclib monotherapy showed modest response
568 with stable disease in 50% of the patients[53]. Partial response to CDK4 inhibitor in a subset of lung
569 cancer patients warranted an exploration of combination with other targeted therapies to achieve
570 durable response. Zhou et al.[54] demonstrated a synergistic growth inhibition in *KRAS* and
571 *CDKN2A* mutant NSCLC xenografts with AZD6244 and palbociclib. Ongoing phase I/II clinical
572 trials (NCT03170206 and NCT02022982) in advanced K-Ras driven NSCLC patients are
573 investigating the combinatorial effect of MEK and CDK4 inhibitors. Additionally, the combination
574 of CDK4 and MAPK pathway inhibitors have shown tumor regression in multiple other cancer
575 types utilizing xenografts models, especially with *KRAS*, *NRAS* or *BRAF* mutations[30]. BRAF- and
576 NRAS-mutant melanoma are particularly receptive to combinatorial therapy[55-58] and phase I
577 clinical studies have shown promising activity in these tumor types as well[59]. Clinical trials are
578 currently investigating BRAF and MEK inhibitors in combination with ribociclib in BRAF-mutant
579 melanoma and other solid tumors with BRAFV600 mutations[60]. In K-Ras mutant colon cancer,
580 monotherapy with either MEK or CDK4 inhibitors has been disappointing[61,62]; however synergistic
581 effects were observed in xenograft models of K-Ras mutant colorectal cancer upon treatment with
582 a combination[38,63], which led to a phase II clinical trial in *KRAS*- or *NRAS*-mutant colorectal cancer
583 patients testing binimetinib and palbociclib in combination[60]. Not only are the two therapies
584 synergistic, but studies have also shown that CDK4 inhibitors are able to overcome MEK inhibitor
585 resistance[64] and vice versa[65]. These findings are corroborated by our results in the present study
586 demonstrating the efficacy of CDK4 and MEK inhibitors.

Results in our immunocompetent syngeneic models will allow us to further extend our investigation into effects on the immune microenvironment. Evidence from past studies indicated that CDK4 depletion reduced infiltration of CD4+ FoxP3+ Tregs[66] and CDK4 inhibitors increased tumour immunogenicity and cytotoxic T-cell mediated clearance of tumor cells[67]. CDK4 inhibitors also enhanced effector T-cell infiltration and activation [68]. Additionally, PD-L1 degradation stability was shown to be regulated by CDK4 through cullin 3–SPOP E3 ligase via proteasome-mediated degradation which primed the tumors for effective response to combination treatment with CDK4 inhibitor and PD-1-PD-L1 immune checkpoint blockade[69]. Other investigations revealed that PD-L1 expression was modulated RB-NF-κB axis which could be exploited to overcome cancer immune evasion triggered by conventional or targeted therapies[70]. Combination of CDK4 and MEK inhibitor induced a senescence-associated secretory phenotype (SASP) that provoked a natural killer cell surveillance program and resulted in tumor cell death[71].

The application of combinatorial treatments with MEK and CDK4 inhibitors in multiple pre-clinical *in vitro* (dual fluorescent sensor system, 3D assays) and *in vivo* models (syngeneic and autochthonous mouse models) effectively prevented outgrowth of resistant tumor subpopulations and was significantly better than either monotherapy. Such findings demonstrate that CDK4 and MAPK pathway are intertwined in lung cancer progression and durable response can be attained if these pathways are targeted judiciously. Fighting cancer at two fronts: by interfering with two distinct regulatory networks and targeting tumor subpopulations should benefit patients and help to prevent resistance development. Additionally, timing of administration of drugs may be an important criteria to consider where a sequential regimen could provide improved targeting of tumor subpopulations that arise due to tumor plasticity.

Methods

shRNA screens

Murine lung cancer cell lines (393P and 344P) were infected at a multiplicity-of-infection (MOI) of 0.3 with a pooled shRNA lentiviral library targeting genes associated with known kinase activity (10 shRNA/gene, for target list and shRNA sequences see Table S2 and S4). Parallel *in vivo* and *in vitro* screens were performed, and the shRNA-coupled barcodes were detected by high-throughput sequencing technology [for detailed procedures and primer sequences see[72]]. *In vivo* and *in vitro* screens were carried out in triplicate and duplicate, respectively. Raw counts for the screen endpoints and a reference population, isolated after transduction, were normalized using the variance stabilizing transformation with the DESeq2 in R. The normalized counts were divided by the reference cells that were isolated immediately following transduction to estimate a fold change in barcode abundance. Four independent shRNAs targeting essential genes (*RPL30, PSMA1*) or luciferase (LUC) were cloned with 5 unique barcodes each and incorporated in the library as positive and negative controls (20 reagents/control, see Table S1 and S3). One *LUC* hairpin showed apparent off-target effect, which has been observed over a wide-spectrum of *in vitro* and *in vivo* screens. One hairpin for *PSMA1* did not show robust drop out, and this pattern was consistent across the 5 barcodes, indicating that this result was not reflective of poor screen performance. The separation of positive and negative controls was evaluated by the robust strictly standardized mean (SSM, Table S1 and S3), excluding the hairpins mentioned above. Fold change distribution was converted to percentiles, and biological replicates were collapsed for RSA analysis. The RSA logP-values and ranks are provided in Tables S2 and S4.

Immunoprecipitation assay

Cells were washed twice with PBS on ice, scraped and pelleted. Supernatant was removed and the pellet was lysed in 500 µl lysis buffer [150 mM NaCl, 50 mM Tris-HCl (pH 7.5), 0.5% NP-40, 50 mM NaF, 1 mM Na orthovanate, 1 mM *β*-glycerophosphate, 10% glycerol, PMSF and protease inhibitor] and incubated on ice for 30 min. Samples were sonicated for 1 min and centrifuged at 13,000 rpm for 10 min. The supernatant was collected and precleared for 1 hourat

636 4^{O}C with non-specific IgG and protein A/G agarose beads. Dynabeads were incubated for 1h with
637 2µg of antibody at 4°C on a rotating platform. 500 µg of pre-cleared lysate was subjected to
638 immunoprecipitation overnight at 4°C. Antibody-antigen complexes were washed with lysis buffer
639 and then eluted with 2x SDS sample Buffer at 100^{O}C and analyzed by western blot.

640 *Chromatin Immunoprecipitation (ChIP)*

641 Cells were cross-linked with 1% formaldehyde at room temperature for 10 min. Glycine
642 was added to a final concentration of 0.125 M for 5 min at room temperature. Cells were then
643 washed with PBS with protease inhibitor, scraped and centrifuged (12,000 rpm, 4^{O}C for 2 min).
644 The supernatant was removed and the pellet was resuspended in 1 ml of lysis buffer [50mM Tris-
645 HCl (pH 8.1), 10mM EDTA, 1% SDS, protease inhibitor] incubated on ice for 10 min. Samples
646 were sonicated on ice for 30 cycles at 50% amplitude with 5 seconds pulse intervals and 10
647 seconds rest intervals. Supernatants were recovered by centrifugation at 12,000 rpm for 5 min.
648 Lysates are diluted 1:10 in ChIP dilution buffer [16.7 mM Tris-HCl (pH 8.1), 16.7 mM NaCl, 1.2
649 mM EDTA, 0.01% SDS, 1.1% Triton X-100, protease inhibitor]. Sheared DNA was precleared
650 with 2 µg sheared salmon sperm DNA and 30 µL protein A/G beads (sc-2003) at 4^{O}C for 1 hour
651 with rotation. Beads were pelleted, the supernatant was collected and an aliquot (1/20th) of the
652 chromatin preparation was set aside and designated as the Input Fraction. The rest of the sample
653 was divided into parts for incubation with 2 µg rabbit IgG (sc-2027) and ZEB1 (santacruz)
654 antibodies overnight at 4^{O}C with rotation. The immune complexes were captured the next day by
655 incubation with 30 µL of pre-cleared beads and 2 µg sheared salmon sperm DNA for 2 h at 4^{O}C.
656 Beads were pelleted by centrifugation for 1 min at 4^{O}C at 100 g and washed sequentially for 10
657 min at 4^{o}C with rotation with 1 ml of the following buffers: low salt wash buffer [20 mM Tris-HCl
658 (pH 8.1), 150 mM NaCl, 2 mM EDTA, 1% Triton X-100, 0.1% SDS]; high salt wash buffer [20 mM
659 Tris-HCl (pH 8.1), 500 mM NaCl, 2 mM EDTA, 1% Triton X-100, 0.1% SDS]; LiCl wash buffer [10
660 mM Tris-HCl (pH 8.1), 1 mM EDTA, 1% sodium deoxycholate, 1% NP-40, 0.25 mM LiCl]. Finally,

the beads were washed twice with 1 ml TE buffer [1 mM EDTA, 10 mM Tris–HCl (pH 8.0)] for 5 min at 4^{O}C. The immuno-complexes were then eluted in 120 µl elution buffer [1% SDS, 100 mM NaHCO3] for 15 min with rotation at room temperature. Reverse cross-linking was done by adding NaCl to the final concentration of 200 mM to ChIP and input samples and incubating at 65^{O}C for 6 hrs. This followed by treatment with RNAase and proteinase K (40 µg/ml) incubating for 1 hourat 45^{O}C. DNA was purified using QIAquick PCR Purification Kit (Qiagen), and 50 ng of eluted DNA was used for each qPCR reaction with primers listed in Table S10 to quantify relative ChIP signal.

Synergy determination

The Chou-Talalay method was used to determine possible synergistic effects between inhibitors[26]. Compusyn software (ComboSyn Inc.) was used to determine synergy between drug combinations. Drug-drug interactions were analyzed based on combination index whereby interactions can be additive (CI=1), antagonistic (CI>1), or synergistic (CI<1). Drug concentrations in the combination were compared to the amount of drug alone required to reach same effects. This is expressed as the dose reduction index, DRI. The amounts of drugs in each combination were pre-determined from each inhibitors IC50 values and inhibitors were assayed in defined dilution series and at a constant ratio.

Animal studies

All animal experiments were reviewed and approved by the Institutional Animal Care and Use Committee (IACUC) at The University of Texas MD Anderson Cancer Center. All mice used in the studies were immunocompetent and assessed for health daily by the Department of Veterinary Medicine and Surgery (DVMS). All mice were genotyped to determine the mutational status by tail snips 2 weeks after birth. For *in vivo* tumor growth assays with transplantation of mouse lung cancer cell lines, male and female wild-type 129/Sv mice ages 3 months and up were

used. Cells were implanted subcutaneously into the right flanks of 129/Sv mice and allowed to form tumors for 2 to 3 weeks, at which point tumor volumes were approximately 150 to 200 mm^3 measured using digital calipers. For conditional mouse models of lung adenocarcinoma (*Kras*$^{LSL/+}$, *Kras*$^{LSL/+}$*p53*$^{flox/flox}$ and *Kras*$^{LSL/+}$*miR-200c*$^{-/-}$) (previously describes in ref.[11]), adenovirus-expressing Cre recombinase was administered into mouse lungs at 3 months of age by intratracheal intubation at a viral titer of $2.5x10^7$ viruses per mouse. Mice were housed specifically in suites designated for biohazard handling as approved under the IACUC protocol. Two weeks post-infection, mice were returned to the regular housing suite. At 3 months post-induction, mouse lungs were visualized by micro-CT scans to confirm tumor formation and measure tumor areas. For drug treatment experiments, mice were randomized to either treatment or vehicle control groups AZD6244 (Selleckchem) and palbociclib (MedChemExpress) were administered daily by oral gavage at a dosage of 25 mg/kg mouse weight and 50 mg/kg mouse weight, respectively. Tumor sizes were measured weekly after treatment began. AZD6244 was dissolved at 5 mg/mL in solvent (4% DMSO, 30% PEG 300, 5% Tween 80), and palbociclib was dissolved at 10 mg/mL in solvent (Lactic acid buffer (50 mM, pH 4.0)). Control mice received solvent at a volume equal to the drug dosage at the indicated drug concentrations. Mouse weights were measured weekly to adjust total dosage and assess the effects of drug combinations on mouse health. After euthanasia by CO_2 exposure at 3 L/min, syngeneic primary tumors and/or mouse lungs were formalin-fixed, paraffin-embedded, and sectioned for histological analysis.

Bliss model for tumor models

In vivo combination synergy analysis was done using the method of Bliss Independence as previously described[30]. A primary analysis day was specified for each study, usually at or near the last day of treatment. On that day, the expected additive response (EAR) tumor volume for the combination group was defined, per the Bliss method, as $EAR=(V_1*V_2)/V_C$, where V_1 and V_2 are the mean tumor volumes in the single-agent groups, and V_C is the mean

volume in the control group. Next, the control group tumor volume change from baseline was defined as $\Delta V = V_C - V_0$. Then an additive range around the EAR was defined, via upper and lower limits, as EAR_U = min(2*EAR, EAR + 0.15*dV) and EAR_L=max(EAR/2,EAR-0.15*dV). If the observed mean combination volume on that day was larger than the mean volume of either single agent, the combination was called antagonistic. If it was smaller than that but larger than EAR_U, the combination was called less than additive. If it was between EAR_U and EAR_L, then the combination was called additive; otherwise, the combination was called synergistic.

Statistical analysis

Statistical analysis was carried out as described in each corresponding figure legend. A p-value of <0.05 was considered statistically significant. Data are presented as mean ± SD unless otherwise noted. All analyses were performed in GraphPad Prism software (version 8).

Figure Legends

Fig 1: Mesenchymal lung cancer cells exhibit increased dependency on CDK4 for growth. **(A)** Schematic illustration of the workflow of the shRNA dropout screens. A library of lentiviral particles expressing 10 different barcoded shRNAs was transduced into murine KP mutant lung cancer cells. The cells were cultured *in vitro* or implanted in nude or syngeneic 129/Sv mice and later sequenced for barcoded shRNAs and compared to reference cells. **(B)** Results from Kinome and FDAome shRNA dropout screens in 393P (epithelial) and 344P (mesenchymal) cell lines and tumors compared based on the redundant shRNA activity (RSA). Top differential hits are labeled on the graphs, most important being CDK4 (red). Venn diagram shows comparisons across different conditions and top hits identified. **(C)** Cluster plot analysis of Spearman's rank correlation between EMT score and CDK4 mRNA expression of 118 human NSCLC cell lines. **(D)** *In vitro cell* viability after 48 hour palbociclib treatment in a panel of epithelial and mesenchymal murine (393P, 344SQ) and human (H358, H1299) lung cancer cell lines. n=8 per drug concentration. The curve was generated using a nonlinear regression fit model. **(E)** Western blot showing the effect on signaling in 393P and 344SQ tumor cells upon treatment with abemaciclib (A: 2 μM) and ribociclib (R: 2 μM) for 24 and 48 hours. **(F)** Top: Relative mRNA expression of CDK4 upon doxycycline mediated induction of shRNAs targeting CDK4 at 72 hours. Bottom: Growth rates of 393P and 344SQ cells with or without CDK4 knockdown over 72 hours measured by MTT assay. One and two-way ANOVA test was used for statistical analysis, respectively. **(G)** Western blot analysis of CDK4 pathway after 72 hours of CDK4 knockdown. **** $p<0.0001$; ** $p<0.001$.

Fig 2: The CDK4 pathway is dynamically regulated by the EMT status of tumor cells (A) Cell cycle analysis 393P and 344SQ cells using propidium iodide (PI). Baseline cell cycle was determined by staining cells in culture with PI. Cell cycle arrest was induced by serum starvation of cells for 24 hours followed by release into cell cycle by addition of FBS containing media and analyzed after 10, 20 and 36 hours. **(B)** Subcellular fractionation followed by western blot analysis of indicated cell cycle markers. **(C)** Top: Representative images of immunofluorescence on 393P and 344SQ wild type cells for indicated markers. Scale bar: 50 μM. Bottom: 4-6 biological replicates were analyzed for quantification of the fluorescent signal. One-way ANOVA was used for statistical analysis. **(D-E)** Western blot analysis of murine (D) and human (E) cells with ZEB1 and miR-200 expression. Cells were induced with 2 μg/ml of doxycycline for times indicated. **(F)** Immunohistochemistry on tumors derived from 393P, 344SQ and 393P_AZD^{R} tumors for indicated markers. Scale bar: 50 μM **(G)** Western blot analysis on cell lines derived from 393P tumors treated with vehicle or AZD6244 for indicated markers. **(H)** *In vitro* cell viability assay on 393P, 344SQ, 393P_vehicle and 393P_AZD^{R} after 48 hours of AZD6244 and palbociclib treatment. n=8 per drug concentration. The curve was generated using a nonlinear regression fit model. **** $p<0.0001$; *** $p<0.005$; ** $p<0.001$.

Fig 3: ZEB1 regulates p21 expression and causes differential CDK4 pathway activation. (A) Transient knockdown of p21 and p27 using 20 nM si-RNAs for 48 hours in 393P and 344SQ cells followed by western blot analysis. **(B)** (Left) Immunofluroscent staining of 393P, 393P_AZD^R and 344SQ cells. Scale bar top: 100 μM, bottom: 10 μM. (Right) Quantification of cells co-staining positive for CDK4 and p21 in each cell lines. 4-6 biological replicates were analyzed for quantification of the fluorescent signal. **(C)** Relative expression of *Cdkn1a* mRNA in a panel of epithelial and mesenchymal murine lung cancer cells (left) and 393P vehicle and AZD^R cell lines (right). **(D)** Cluster plot analysis of Pearson's correlation between *CDKN1A* mRNA and EMT score in 29 KRAS mutant human lung adenocarcinoma cell lines. **(E)** Immunohistochemistry on tumors derived from 393P, 344SQ and 393P-AZD^R cells Scale bar: 50 μM. **(F)** Cluster plot analysis of Pearson's correlation between ZEB1 and p21 H scores in NSCLC specimens. **(G and H)** Relative expression of *Cdkn1a* mRNA and p21 protein levels upon induction of EMT or MET. ZEB1 induction for 48 hours with 2 μg/ml of doxycycline in murine (G, top) and human (G, bottom) epithelial lung cancer cell lines. miR-200 induction for 48 hours with 2 μg/ml of doxycycline in murine (H, top) and human (H, bottom) mesenchymal lung cancer cell lines. **(I)** Luciferase reporter assay to determine relative luciferase activity of CDKN1A promoter reporter construct transfected into epithelial H358 and H441 cells with induced ZEB1 expression or mesenchymal H1299 with induced miR-200 expression. Relative luciferin signal was normalized to promoter-less vector control signal. **(J)** Fold enrichment by qPCR analysis of CDKN1A promoter containing ZEB1 binding site after endogenous ZEB1 ChIP in H441 cells with inducible ZEB1 expression or H1299 cells with inducible miR-200 expression, using ZEB1 antibody or immunoglobulin G (IgG) control antibody. One-way ANOVA was used for statistical analysis in all the panels. **** $p<0.0001$; *** $p<0.005$; ** $p<0.001$; * $p< 0.05$; ns: not significant.

Fig 4: Suppression of p21 in mesenchymal cells regulates CDK4 pathway. (A) Transient knockdown of CDK4 using 20 nM si-RNAs for 12, 24 and 48 hours in epithelial and mesenchymal cancer cells followed by western blot analysis. **(B)** (Left) Graphical representation of the differences in CDK4-p21 complex formation in epithelial and mesenchymal cancer cells. (Right) Co-IP of endogenous CDK4 and p21 in epithelial (393P and 344SQ_miR-200) and mesenchymal (344SQ and 344SQ_vec) cell lines and analyzed by western blot with anti-CDK4 and anti-p21 antibodies. **(C)** Constitutive overexpression of *Cdkn1a* in 344SQ cell lines. Relative mRNA expression of *Cdkn1a* (left), western blot analysis of CDK4 pathway (middle) and co-IP of CDK4 and p21 in 344SQ cells (right). **(D)** Growth rates of 344SQ cells ± p21 constitutive overexpression over 4 days measured by WST-1 assay. **(E)** Tumor volume measurements at indicated time points of 344SQ tumors ± p21 (n= 5 per group). Data are presented as mean ± SEM. **(F)** Doxycycline induced overexpression of *Cdkn1a* in 344SQ cell lines for 48 hours. Relative mRNA expression of *Cdkn1a* (left), western blot analysis of CDK4 pathway (middle) and co-IP of CDK4 and p21 in 344SQ cells (right). **(G)** Growth rates of 344SQ cells ± p21 overexpression (doxycycline induced) over 4 days measured by WST-1 assay. **(H)** Tumor volume measurements at indicated time points of 344SQ tumors ± p21 expression with doxycycline feed (n=9-10/group). Dox feed was started after tumors reached a size of 100-150 mm^3 (indicated by arrow). Data are presented as mean ± SEM. **(I)** Western blot of EMT markers with CDK4 knockdown for 72 hours. **(J)** *In vitro* cell viability assay on 344SQ (top) and 344P (bottom) lung cancer cell lines with or without transient knockdown of CDK4 and treatment with a range of concentrations of AZD6244 for 48 hours. n=8 per drug concentration. The curve was generated using a nonlinear regression fit model. **(K)** Palbociclib and AZD6244 were used to determine the Drug Reduction Index (DRI) and Combination Index (CI) using Chou-Talalay method on 344SQ cells. **(L)** Western blot analysis on cells treated with AZD6244 (5μM) and palbociclib (5μM) for 48 hours. Cleaved caspase-3 was used as an apoptotic marker. Statistical analysis for *C, E, F and H*: Unpaired t-test and for *D* and *G*: Two-way ANOVA test. **** $p<0.0001$; *** $p<0.005$; ** $p<0.001$; * $p< 0.05$.

Fig 5: Co-targeting CDK4 and MAPK pathways targets different tumor cell subsets. (A-B) Apoptosis was determined by annexin V and propidium iodide staining of murine and human lung cancer cells after treatment with AZD6244 (5 μM) or palbociclib (5 μM) for 48 hours. The data are presented as the mean ± SD from three replicates. **(C)** 344SQ_Z-cad cells were treated with DMSO, mocetinostat (1 μM), AZD6244 (5 μM), or palbociclib (5 μM) for 48 hours followed by fluorescent image acquisition. Scale bar: 50 μM. **(D)** Images from (C) were quantified for the percentage of RFP or GFP color pixels calculated per field of view (FOV). n=4-6 FOVs. **(E)** 344SQ_Z-cad cells were treated with DMSO, AZD6244 (5 μM), palbociclib (5 μM) or the combination. NucView® 405 Caspase 3 substrate was added to each condition as a readout for apoptosis. Representative fluorescent images were acquired 48 hours after addition of drugs (left). Scale bar = 25 μM. Arrows indicate apoptotic cells. Images were quantified for total caspase-3+ cells as a percentage of total cells in 4-6 FOVs (right). **(F-G)** *Ex vivo* tumors (EVTs) were plated in a Matrigel (MG) or a Collagen/Matrigel (Coll/MG) matrix. After 24 hours, EVTs were treated with DMSO, AZD6244 (5 μM), palbociclib (5 μM) or the combination. (F) Treatment in MG was continued for 9 days with representative images from last day of the culture shown (left panel, scale bar: 200 μM). Percentage of RFP and GFP color pixels in 4-6 FOVs (middle panel). Data are represented as mean. At the end of the treatment, Cell Titer-Glo reagent was added and relative luciferin signal was measured (right panel). (G) EVTs in Coll/MG matrix were treated for 5 days. Representative images at the end of experiment shown (left panel, scale bar: 100 μM), quantification of percentage RFP and GFP color pixels in 4-6 FOVs (middle panel) and relative luciferin signal using Cell Titer-Glo reagent (right panel). Treatment groups were compared to DMSO using one-way ANOVA in all the panels. **** $p<0.0001$; *** $p<0.005$; ** $p<0.001$; * $p< 0.05$; ns: not significant.

Fig 6: Combination of MEK and CDK4 inhibitors controls syngeneic tumor growth and prevents emergence of EMT mediated resistance. (A) *In vivo* volume measurements at the indicated time points for 344SQ subcutaneous tumors in syngeneic WT mice (n=5 per group) after daily treatment with solvent, AZD6244 (25 mg/kg), palbociclib (50 mg/kg) or combination. Arrow indicates start of the treatment. **(B)** 344SQ subcutaneous tumors were treated with solvent (n=5), AZD6244 (25 mg/kg) (n=10), palbociclib (50 mg/kg) (n=10) or combination (n=5) for 7 weeks at which point resistance to palbociclib emerged. 5 mice from palbociclib treatment alone arm were converted to combination arm and treatment was continued for another 3 weeks (marked by purple X). **(C)** Fold change in 344SQ tumors in the palbociclib and combo arms over 13 weeks. **(D)** Immunohistochemical analysis on 344SQ tumors treated with solvent or palbociclib for 7 weeks with indicated markers. Scale bar: 50 μM. **(E)** *In vivo* volume measurements at indicated time points for 393P subcutaneous tumors in syngeneic WT mice (n=5 per group) after daily treatment with solvent, AZD6244 (25 mg/kg), palbociclib (50 mg/kg) or combination. Arrow indicates start of treatment. **(F)** *In vivo* volume measurements of 393P-AZD^{R} subcutaneous tumors in syngeneic WT mice (n=5 per group) after daily treatment with AZD6244 (25 mg/kg) or palbociclib (50 mg/kg). Arrow indicates start of treatment at day 14. **(G)** IHC analysis on 344SQ and 393P tumors harvested from (A) and (E) respectively, with indicated markers. Scale bar: 50 μM. **(H-J)** Tumors from the experiments described in (A) and (E) were stained with Ki67 and TUNEL assay to measure cell proliferation and cell death respectively. Representative IHC images are shown in (H). Scale bar: 50 μM. Images were quantified for Ki67 (I) and TUNEL (J) staining in each treatment group. n=2-3 per group with 3-6 FOV per mouse. Statistical significance was determined by one-way ANOVA in all the panels. **** $p<0.0001$; *** $p<0.005$; ** $p<0.001$; * $p< 0.05$; ns: not significant.

Fig 7: Concomitant targeting of CDK4 and MAPK pathways augments response in Kras mutant autochthonous lung tumors. (A) Immunohistochemistry for indicated markers on *Kras*$^{LSL/+}$, *Kras*$^{LSL/+}$*P*$^{flox/flox}$ and *Kras*$^{LSL/+}$*M*$^{-/-}$ lung sections 18-20 weeks post Ad-Cre infection. Scale bar: 50 μM. **(B)** Immunohistochemistry for indicated markers on *Kras*$^{LSL/+}$, *Kras*$^{LSL/+}$*P*$^{flox/flox}$ and *Kras*$^{LSL/+}$*M*$^{-/-}$ lung sections 18-20 weeks post Ad-Cre infection. Scale bar: 50 μM. **(C)** Percentage change in overall lung tumor area of *Kras*$^{LSL/+}$, *Kras*$^{LSL/+}$*P*$^{flox/flox}$ and *Kras*$^{LSL/+}$*M*$^{-/-}$ mice after 6-8 weeks of daily treatment with AZD6244 (25 mg/kg), palbociclib (50 mg/kg) or both as assessed by micro-CT imaging of mouse lungs. Significance was determined using Brown-Forsythe and Welch ANOVA tests. **(D and E)** Immunohistochemistry for indicated markers on lung sections from mice treated Kras$^{LSL/+}$P$^{flox/flox}$ (D) and Kras$^{LSL/+}$M$^{-/-}$ (E) treated with AZD6244 and palbociclib for 6-8 weeks. Scale bar: 50 μM. **(F)** Proposed working model demonstrating differential CDK4 and MAPK signaling pathway activation and sensitivity to CDK4 and MEK inhibitor treatments between epithelial and mesenchymal lung cancer cells due to ZEB1 regulation of p21 expression.

Table 1. IC50 of epithelial and mesenchymal cell lines for indicated CDK4 inhibitors as determined by viability assay.

CDK4 inhibitor	Epithelial cells	IC50	Mesenchymal cells	IC50
Palbociclib	393P	10.8	344SQ	2.2
	393P_Vector	5.2	393P_ZEB1	0.6
	344SQ_miR-200	5.2	344SQ_Vector	0.8
	H358	9.6	A549	1.1
	H441	10	H1299	0.5
	H441_Vector	16	H441_ZEB1	2.6
	H1299_miR-200	3	H1299_Vector	0.6
Abemaciclib	393P	15	344SQ	2.2
	H358	1	H1299	0.2
Ribociclib	393P	19.2	344SQ	3.8
	H358	29	H1299	3.3

Author Contributions

AP and DLG conceived the project and designed experiments. AP wrote the manuscript and performed and/or assisted in all experiments and data analyses. JMK generated p21 overexpression and knockdown cell lines. BLR assisted with flow cytometry analysis. AP and JJF generated the adeno-Cre–induced mouse lung tumors. BLR and JJF assisted with the animal studies. JKO assisted with IHC staining of murine tissues. LD and JW performed bioinformatics analyses on the RPPA dataset and human lung cancer cell line panels. RM and AC executed functional genomics screens. CAB processed and analyzed deep sequencing barcode data. WL and LSS performed IHC on human lung cancer specimens and HB performed digital image analysis. MGR provided overall supervision for IHC staining. DLG supervised and oversaw all aspects of the project and the writing of the manuscript.

Acknowledgments

This work was supported in part by National Institutes of Health grants R37CA214609 (D.L.G.), F32CA239292 (J.M.K.) and CPRIT MIRA RP160652-P3 (D.L.G.). This work was also supported in part by the University of Texas Lung Cancer SPORE grant P50-CA070907, the LUNGevity foundation award (D.L.G.), Rexanna's Foundation (D.L.G.), and through generous philanthropic contributions to The University of Texas MD Anderson Lung Cancer Moonshot Program. The Flow Cytometry Lab South Campus Core facility at MDACC is supported by CCSG NCI P30 CA16672. We thank Dr. Jonathan M. Kurie (MD Anderson Cancer Center, Houston TX) for providing $Kras^{G12D}$ mutant (K1) and $Kras^{G12D}/p21^{-/-}$ (KC3 and KC4) cell lines.

References

1 Sharma, S. V., Haber, D. A. & Settleman, J. Cell line-based platforms to evaluate the therapeutic efficacy of candidate anticancer agents. *Nature reviews cancer* **10**, 241-253 (2010).

2 Herbst, R. S., Heymach, J. V. & Lippman, S. M. Lung cancer. *The New England journal of medicine* **359**, 1367-1380, doi:10.1056/NEJMra0802714 (2008).

3 Mascaux, C. *et al.* The role of RAS oncogene in survival of patients with lung cancer: a systematic review of the literature with meta-analysis. *British journal of cancer* **92**, 131-139, doi:10.1038/sj.bjc.6602258 (2005).

4 Siegel, R. L., Miller, K. D. & Jemal, A. Cancer statistics, 2020. *CA: a cancer journal for clinicians* **70**, 7-30 (2020).

5 Cox, A. D., Fesik, S. W., Kimmelman, A. C., Luo, J. & Der, C. J. Drugging the undruggable RAS: Mission possible? *Nature reviews. Drug discovery* **13**, 828-851, doi:10.1038/nrd4389 (2014).

6 Hong, D. S. *et al.* KRASG12C inhibition with sotorasib in advanced solid tumors. *New England Journal of Medicine* **383**, 1207-1217 (2020).

7 Jänne, P. A. *et al.* Selumetinib plus docetaxel compared with docetaxel alone and progression-free survival in patients with kras-mutant advanced non–small cell lung cancer: the select-1 randomized clinical trial. *Jama* **317**, 1844-1853 (2017).

8 Blumenschein, G. R., Jr. *et al.* A randomized phase II study of the MEK1/MEK2 inhibitor trametinib (GSK1120212) compared with docetaxel in KRAS-mutant advanced non-small-cell lung cancer (NSCLC)†. *Annals of oncology : official journal of the European Society for Medical Oncology* **26**, 894-901, doi:10.1093/annonc/mdv072 (2015).

9 Singh, A. *et al.* A gene expression signature associated with "K-Ras addiction" reveals regulators of EMT and tumor cell survival. *Cancer cell* **15**, 489-500, doi:10.1016/j.ccr.2009.03.022 (2009).

10 Gibbons, D. L. *et al.* Contextual extracellular cues promote tumor cell EMT and metastasis by regulating miR-200 family expression. *Genes Dev* **23**, 2140-2151, doi:10.1101/gad.1820209 (2009).

11 Peng, D. H. *et al.* ZEB1 suppression sensitizes KRAS mutant cancers to MEK inhibition by an IL17RD-dependent mechanism. *Sci Transl Med* **11**, doi:10.1126/scitranslmed.aaq1238 (2019).

12 Konen, J. M. *et al.* Dual inhibition of MEK and AXL targets tumor cell heterogeneity and prevents resistant outgrowth mediated by the epithelial-to-mesenchymal transition in NSCLC. *Cancer Research*, canres.1895.2020, doi:10.1158/0008-5472.Can-20-1895 (2021).

13 Rubin, S. M., Sage, J. & Skotheim, J. M. Integrating Old and New Paradigms of G1/S Control. *Mol Cell* **80**, 183-192, doi:10.1016/j.molcel.2020.08.020 (2020).

14 Otto, T. & Sicinski, P. Cell cycle proteins as promising targets in cancer therapy. *Nature Reviews Cancer* **17**, 93-115, doi:10.1038/nrc.2016.138 (2017).

15 Bouclier, C. *et al.* Stapled peptide targeting the CDK4/Cyclin D interface combined with Abemaciclib inhibits KRAS mutant lung cancer growth. *Theranostics* **10**, 2008-2028, doi:10.7150/thno.40971 (2020).

16 Esteban-Burgos, L. *et al.* Tumor regression and resistance mechanisms upon CDK4 and RAF1 inactivation in KRAS/P53 mutant lung adenocarcinomas. *Proceedings of the National Academy of Sciences* **117**, 24415-24426, doi:10.1073/pnas.2002520117 (2020).

17 Puyol, M. *et al.* A synthetic lethal interaction between K-Ras oncogenes and Cdk4 unveils a therapeutic strategy for non-small cell lung carcinoma. *Cancer cell* **18**, 63-73, doi:10.1016/j.ccr.2010.05.025 (2010).

18 Nilsson, M. B. *et al.* A YAP/FOXM1 axis mediates EMT-associated EGFR inhibitor resistance and increased expression of spindle assembly checkpoint components. *Sci Transl Med* **12**, doi:10.1126/scitranslmed.aaz4589 (2020).
19 Byers, L. A. *et al.* An epithelial-mesenchymal transition gene signature predicts resistance to EGFR and PI3K inhibitors and identifies Axl as a therapeutic target for overcoming EGFR inhibitor resistance. *Clin Cancer Res* **19**, 279-290, doi:10.1158/1078-0432.CCR-12-1558 (2013).
20 Peng, D. H. *et al.* ZEB1 induces LOXL2-mediated collagen stabilization and deposition in the extracellular matrix to drive lung cancer invasion and metastasis. *Oncogene* **36**, 1925-1938, doi:10.1038/onc.2016.358 (2017).
21 Ungewiss, C. *et al.* The microRNA-200/Zeb1 axis regulates ECM-dependent β1-integrin/FAK signaling, cancer cell invasion and metastasis through CRKL. *Scientific reports* **6**, 18652 (2016).
22 Chen, Y. *et al.* Lysyl hydroxylase 2 induces a collagen cross-link switch in tumor stroma. *The Journal of clinical investigation* **125**, 1147-1162 (2015).
23 Meidhof, S. *et al.* ZEB1-associated drug resistance in cancer cells is reversed by the class I HDAC inhibitor mocetinostat. *EMBO Mol Med* **7**, 831-847, doi:10.15252/emmm.201404396 (2015).
24 Chen, Y. *et al.* ZEB1 regulates multiple oncogenic components involved in uveal melanoma progression. *Scientific reports* **7**, 1-14 (2017).
25 Bisteau, X. *et al.* CDK4 T172 phosphorylation is central in a CDK7-dependent bidirectional CDK4/CDK2 interplay mediated by p21 phosphorylation at the restriction point. *PLoS genetics* **9** (2013).
26 Chou, T.-C. Theoretical Basis, Experimental Design, and Computerized Simulation of Synergism and Antagonism in Drug Combination Studies. *Pharmacological Reviews* **58**, 621-681, doi:10.1124/pr.58.3.10 (2006).
27 Toneff, M. J. *et al.* The Z-cad dual fluorescent sensor detects dynamic changes between the epithelial and mesenchymal cellular states. *BMC Biology* **14**, 47, doi:10.1186/s12915-016-0269-y (2016).
28 Padhye, A. *et al.* A novel ex vivo tumor system identifies Src-mediated invasion and metastasis in mesenchymal tumor cells in non-small cell lung cancer. *Scientific reports* **9**, 1-13 (2019).
29 Muthuswamy, S. K., Li, D., Lelievre, S., Bissell, M. J. & Brugge, J. S. ErbB2, but not ErbB1, reinitiates proliferation and induces luminal repopulation in epithelial acini. *Nature cell biology* **3**, 785-792 (2001).
30 Chen, S. H. *et al.* RAF inhibitor LY3009120 sensitizes RAS or BRAF mutant cancer to CDK4/6 inhibition by abemaciclib via superior inhibition of phospho-RB and suppression of cyclin D1. *Oncogene* **37**, 821-832, doi:10.1038/onc.2017.384 (2018).
31 DuPage, M., Dooley, A. L. & Jacks, T. Conditional mouse lung cancer models using adenoviral or lentiviral delivery of Cre recombinase. *Nature Protocols* **4**, 1064-1072, doi:10.1038/nprot.2009.95 (2009).
32 Sherr, C. J. & Roberts, J. M. CDK inhibitors: positive and negative regulators of G1-phase progression. *Genes & development* **13**, 1501-1512 (1999).
33 Walter, D. M. *et al.* RB constrains lineage fidelity and multiple stages of tumour progression and metastasis. *Nature* **569**, 423-427, doi:10.1038/s41586-019-1172-9 (2019).
34 Tarasewicz, E. *et al.* CDK4 inhibition and doxorubicin mediate breast cancer cell apoptosis through Smad3 and survivin. *Cancer biology & therapy* **15**, 1301-1311, doi:10.4161/cbt.29693 (2014).

35 Zelivianski, S., Cooley, A., Kall, R. & Jeruss, J. S. Cyclin-dependent kinase 4-mediated phosphorylation inhibits Smad3 activity in cyclin D-overexpressing breast cancer cells. *Mol Cancer Res* **8**, 1375-1387, doi:10.1158/1541-7786.Mcr-09-0537 (2010).
36 Liu, F. & Korc, M. Cdk4/6 inhibition induces epithelial-mesenchymal transition and enhances invasiveness in pancreatic cancer cells. *Mol Cancer Ther* **11**, 2138-2148, doi:10.1158/1535-7163.Mct-12-0562 (2012).
37 Rencuzogulları, O., Yerlikaya, P. O., Gürkan, A., Arısan, E. D. & Telci, D. Palbociclib, a selective CDK4/6 inhibitor, restricts cell survival and epithelial-mesenchymal transition in Panc-1 and MiaPaCa-2 pancreatic cancer cells. *Journal of cellular biochemistry* **121**, 508-523, doi:10.1002/jcb.29249 (2020).
38 Lee, M. S. *et al.* Efficacy of the combination of MEK and CDK4/6 inhibitors in vitro and in vivo in KRAS mutant colorectal cancer models. *Oncotarget* **7**, 39595-39608, doi:10.18632/oncotarget.9153 (2016).
39 Al Bitar, S. & Gali-Muhtasib, H. The Role of the Cyclin Dependent Kinase Inhibitor p21(cip1/waf1) in Targeting Cancer: Molecular Mechanisms and Novel Therapeutics. *Cancers (Basel)* **11**, 1475, doi:10.3390/cancers11101475 (2019).
40 Xiong, Y. *et al.* p21 is a universal inhibitor of cyclin kinases. *Nature* **366**, 701-704, doi:10.1038/366701a0 (1993).
41 Kreis, N. N., Louwen, F. & Yuan, J. The Multifaceted p21 (Cip1/Waf1/CDKN1A) in Cell Differentiation, Migration and Cancer Therapy. *Cancers (Basel)* **11**, doi:10.3390/cancers11091220 (2019).
42 Guiley, K. Z. *et al.* p27 allosterically activates cyclin-dependent kinase 4 and antagonizes palbociclib inhibition. *Science* **366** (2019).
43 Wilson, A. J. *et al.* Histone deacetylase 3 (HDAC3) and other class I HDACs regulate colon cell maturation and p21 expression and are deregulated in human colon cancer. *The Journal of biological chemistry* **281**, 13548-13558, doi:10.1074/jbc.M510023200 (2006).
44 Manshouri, R. *et al.* ZEB1/NuRD complex suppresses TBC1D2b to stimulate E-cadherin internalization and promote metastasis in lung cancer. *Nature Communications* **10**, 5125, doi:10.1038/s41467-019-12832-z (2019).
45 Fu, R. *et al.* A ZEB1/p53 signaling axis in stromal fibroblasts promotes mammary epithelial tumours. *Nat Commun* **10**, 3210, doi:10.1038/s41467-019-11278-7 (2019).
46 Macleod, K. F. *et al.* p53-dependent and independent expression of p21 during cell growth, differentiation, and DNA damage. *Genes Dev* **9**, 935-944, doi:10.1101/gad.9.8.935 (1995).
47 Sherr, C. J. & McCormick, F. The RB and p53 pathways in cancer. *Cancer cell* **2**, 103-112, doi:10.1016/s1535-6108(02)00102-2 (2002).
48 Otto, T. & Sicinski, P. Cell cycle proteins as promising targets in cancer therapy. *Nat Rev Cancer* **17**, 93-115, doi:10.1038/nrc.2016.138 (2017).
49 Cadoo, K. A., Gucalp, A. & Traina, T. A. Palbociclib: an evidence-based review of its potential in the treatment of breast cancer. *Breast Cancer (Dove Med Press)* **6**, 123-133, doi:10.2147/BCTT.S46725 (2014).
50 Garrido-Castro, A. C. & Goel, S. CDK4/6 Inhibition in Breast Cancer: Mechanisms of Response and Treatment Failure. *Current breast cancer reports* **9**, 26-33, doi:10.1007/s12609-017-0232-0 (2017).
51 Patnaik, A. *et al.* Efficacy and Safety of Abemaciclib, an Inhibitor of CDK4 and CDK6, for Patients with Breast Cancer, Non–Small Cell Lung Cancer, and Other Solid Tumors. *Cancer Discovery* **6**, 740-753, doi:10.1158/2159-8290.Cd-16-0095 (2016).
52 Johnston, S. R. D. *et al.* Abemaciclib Combined With Endocrine Therapy for the Adjuvant Treatment of HR+, HER2−, Node-Positive, High-Risk, Early Breast Cancer (monarchE). *Journal of Clinical Oncology* **38**, 3987-3998, doi:10.1200/jco.20.02514 (2020).

53 Gopalan, P. K. *et al.* A phase II clinical trial of the CDK 4/6 inhibitor palbociclib (PD 0332991) in previously treated, advanced non-small cell lung cancer (NSCLC) patients with inactivated CDKN2A. *Journal of Clinical Oncology* **32**, 8077-8077, doi:10.1200/jco.2014.32.15_suppl.8077 (2014).

54 Zhou, J. *et al.* Palbociclib, a selective CDK4/6 inhibitor, enhances the effect of selumetinib in RAS-driven non-small cell lung cancer. *Cancer Letters* **408**, 130-137, doi:https://doi.org/10.1016/j.canlet.2017.08.031 (2017).

55 Kim, H. S. *et al.* Oncogenic BRAF fusions in mucosal melanomas activate the MAPK pathway and are sensitive to MEK/PI3K inhibition or MEK/CDK4/6 inhibition. *Oncogene* **36**, 3334-3345, doi:10.1038/onc.2016.486 (2017).

56 Kwong, L. N. *et al.* Oncogenic NRAS signaling differentially regulates survival and proliferation in melanoma. *Nature Medicine* **18**, 1503-1510, doi:10.1038/nm.2941 (2012).

57 Li, Z. *et al.* CRISPR Screens Identify Essential Cell Growth Mediators in BRAF Inhibitor-resistant Melanoma. *Genomics, Proteomics & Bioinformatics* **18**, 26-40, doi:https://doi.org/10.1016/j.gpb.2020.02.002 (2020).

58 Ramsdale, R. *et al.* The transcription cofactor c-JUN mediates phenotype switching and BRAF inhibitor resistance in melanoma. *Science Signaling* **8**, ra82-ra82, doi:10.1126/scisignal.aab1111 (2015).

59 Sosman, J. A. *et al.* A phase 1b/2 study of LEE011 in combination with binimetinib (MEK162) in patients with NRAS-mutant melanoma: Early encouraging clinical activity. *Journal of Clinical Oncology* **32**, 9009-9009, doi:10.1200/jco.2014.32.15_suppl.9009 (2014).

60 Scheiblecker, L., Kollmann, K. & Sexl, V. CDK4/6 and MAPK-Crosstalk as Opportunity for Cancer Treatment. *Pharmaceuticals (Basel, Switzerland)* **13**, doi:10.3390/ph13120418 (2020).

61 Infante, J. R. *et al.* Safety, pharmacokinetic, pharmacodynamic, and efficacy data for the oral MEK inhibitor trametinib: a phase 1 dose-escalation trial. *The lancet oncology* **13**, 773-781 (2012).

62 O'Hara, M. H. *et al.* (American Society of Clinical Oncology, 2015).

63 Ziemke, E. K. *et al.* Sensitivity of KRAS-mutant colorectal cancers to combination therapy that cotargets MEK and CDK4/6. *Clinical Cancer Research* **22**, 405-414 (2016).

64 Yadav, V. *et al.* The CDK4/6 Inhibitor LY2835219 Overcomes Vemurafenib Resistance Resulting from MAPK Reactivation and Cyclin D1 Upregulation. *Molecular Cancer Therapeutics* **13**, 2253-2263, doi:10.1158/1535-7163.Mct-14-0257 (2014).

65 de Leeuw, R. *et al.* MAPK Reliance via Acquired CDK4/6 Inhibitor Resistance in Cancer. *Clin Cancer Res* **24**, 4201-4214, doi:10.1158/1078-0432.Ccr-18-0410 (2018).

66 Chow, Y. H. *et al.* Role of Cdk4 in lymphocyte function and allergen response. *Cell Cycle* **9**, 4922-4930 (2010).

67 Goel, S. *et al.* CDK4/6 inhibition triggers anti-tumour immunity. *Nature* **548**, 471-475, doi:10.1038/nature23465 (2017).

68 Deng, J. *et al.* CDK4/6 Inhibition Augments Antitumor Immunity by Enhancing T-cell Activation. *Cancer Discovery* **8**, 216-233, doi:10.1158/2159-8290.Cd-17-0915 (2018).

69 Zhang, J. *et al.* Cyclin D–CDK4 kinase destabilizes PD-L1 via cullin 3–SPOP to control cancer immune surveillance. *Nature* **553**, 91-95, doi:10.1038/nature25015 (2018).

70 Jin, X. *et al.* Phosphorylated RB Promotes Cancer Immunity by Inhibiting NF-κB Activation and PD-L1 Expression. *Molecular Cell* **73**, 22-35.e26, doi:https://doi.org/10.1016/j.molcel.2018.10.034 (2019).

71 Ruscetti, M. *et al.* NK cell-mediated cytotoxicity contributes to tumor control by a cytostatic drug combination. *Science (New York, N.Y.)* **362**, 1416-1422, doi:10.1126/science.aas9090 (2018).

72 Carugo, A. *et al.* In Vivo Functional Platform Targeting Patient-Derived Xenografts Identifies WDR5-Myc Association as a Critical Determinant of Pancreatic Cancer. *Cell Reports* **16**, 133-147, doi:https://doi.org/10.1016/j.celrep.2016.05.063 (2016).

Fig. 1: Mesenchymal lung cancer cells exhibit increased dependency on CDK4 for growth

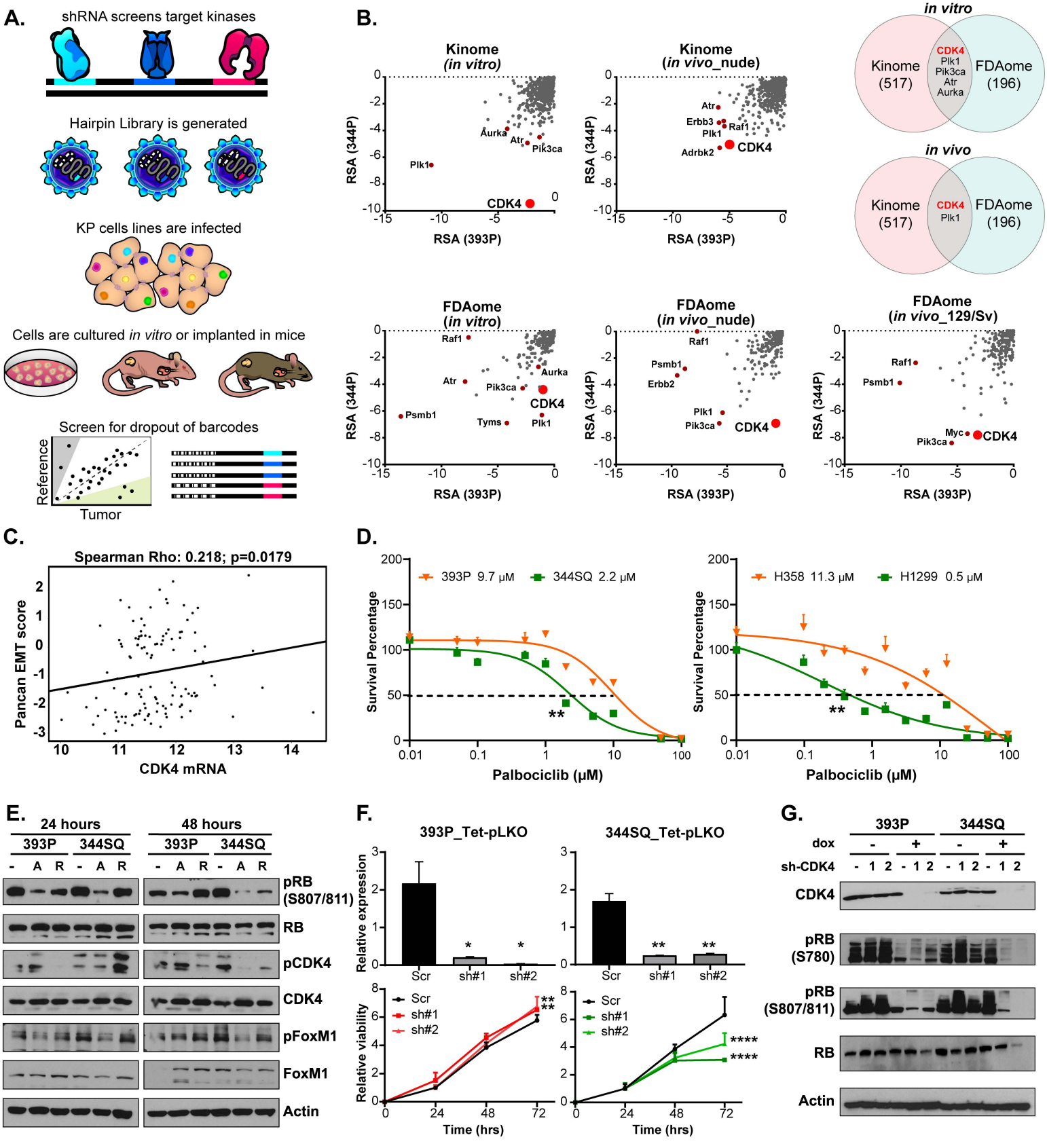

Fig. 2: The CDK4 pathway is dynamically regulated by the EMT status of tumor cells

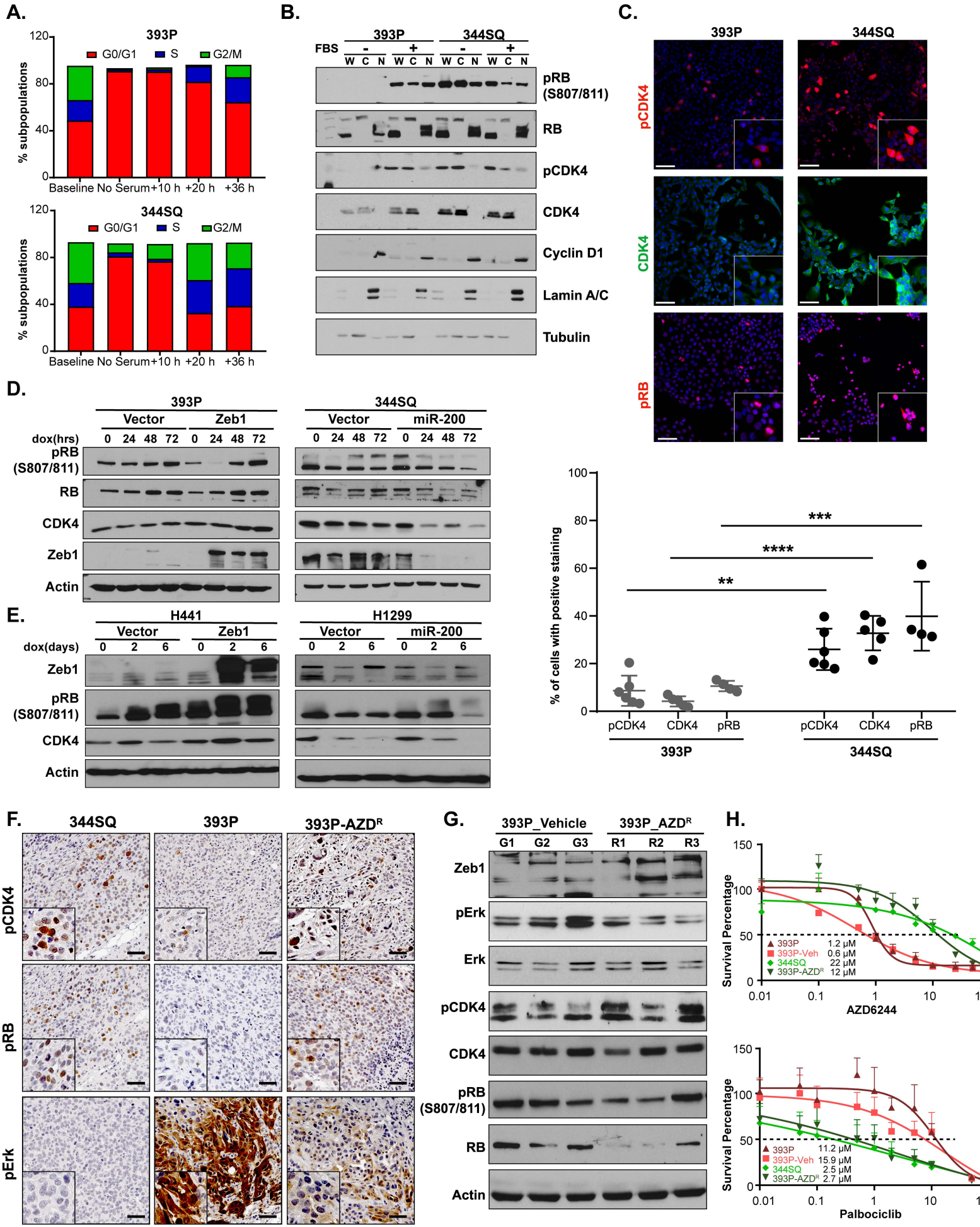

Fig. 3: ZEB1 regulates p21 expression and causes differential CDK4 pathway activation

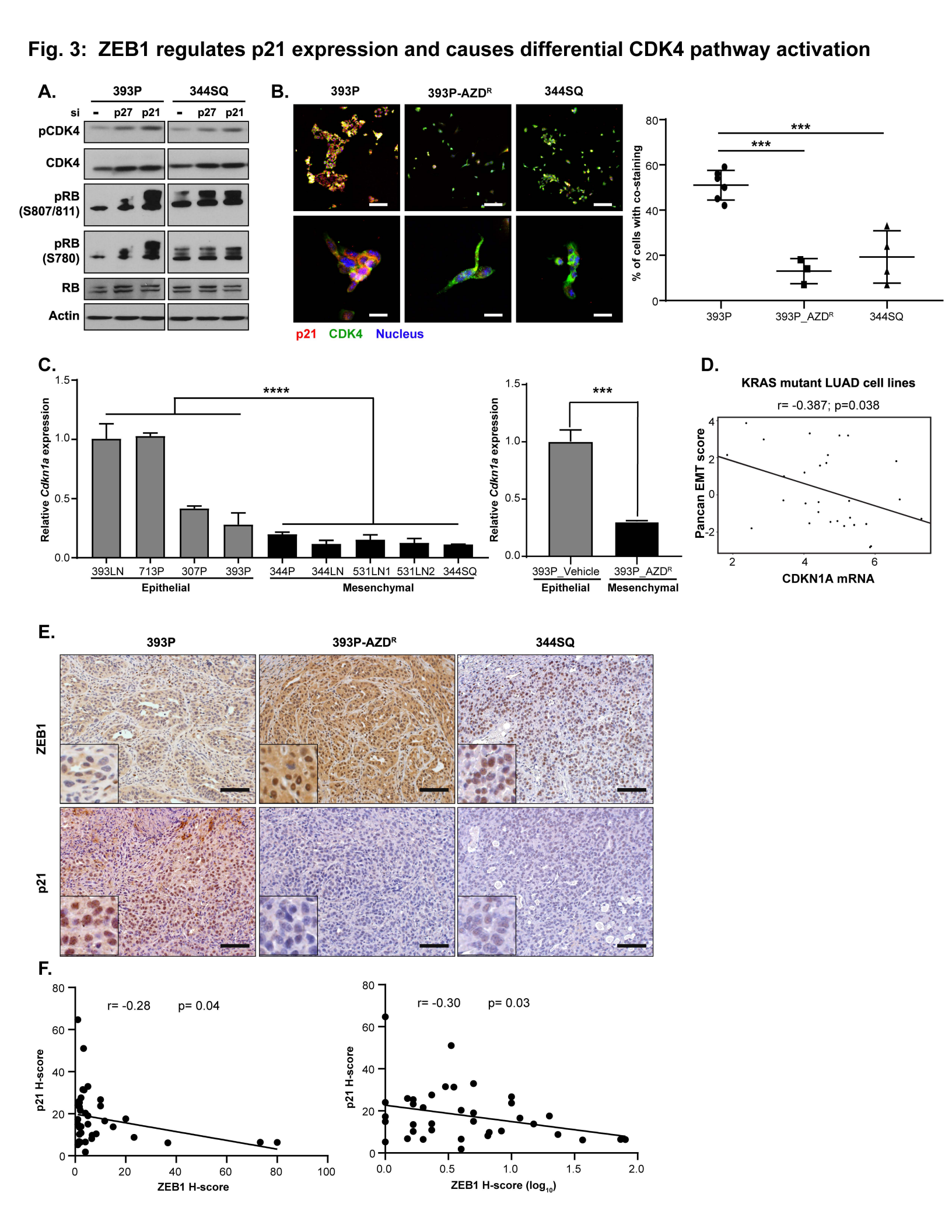

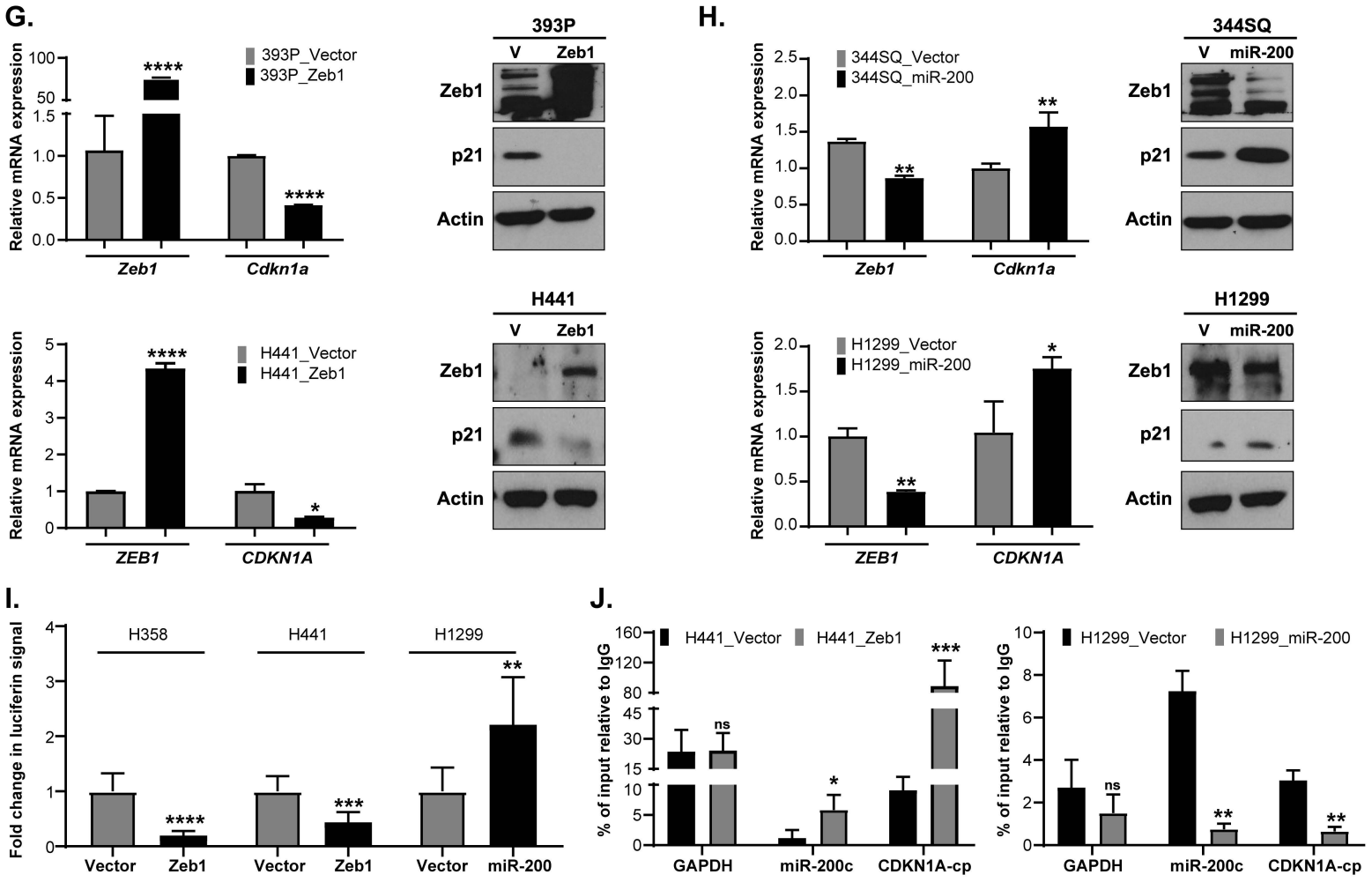
G.
393P
V
Zeb1
393P_Vector
393P_Zeb1
Relative mRNA expression
Zeb1
Cdkn1a
p21
Actin
H441
H441_Vector
H441_Zeb1
ZEB1
CDKN1A
H.
344SQ
miR-200
344SQ_Vector
344SQ_miR-200
H1299
H1299_Vector
H1299_miR-200
I.
Fold change in luciferin signal
H358
H441
H1299
Vector
miR-200
J.
% of input relative to IgG
GAPDH
miR-200c
CDKN1A-cp
ns

Fig. 4: Suppression of p21 in mesenchymal cells regulates CDK4 pathway

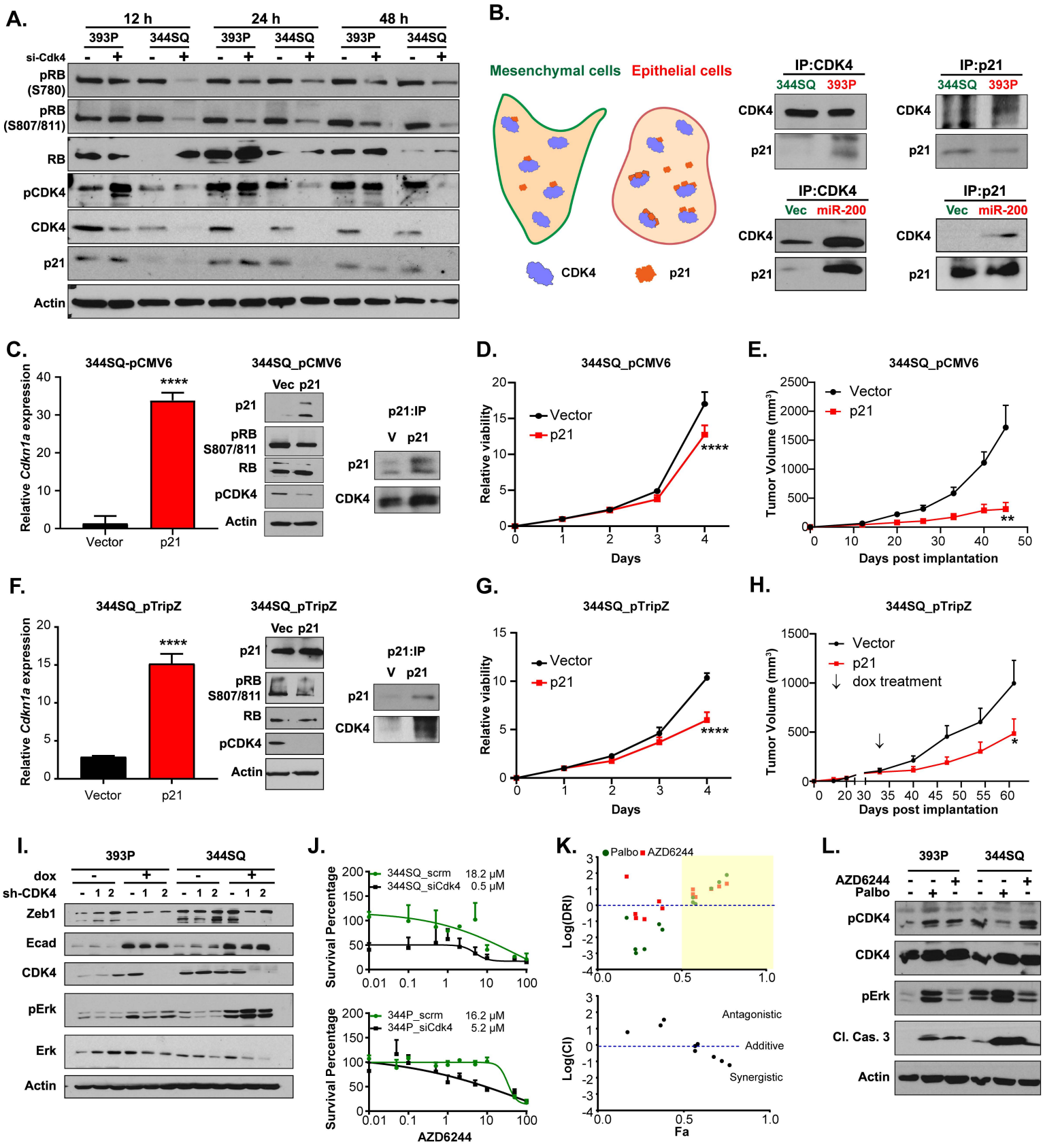

Fig. 5: Co-targeting CDK4 and MAPK pathways targets different tumor cell subsets

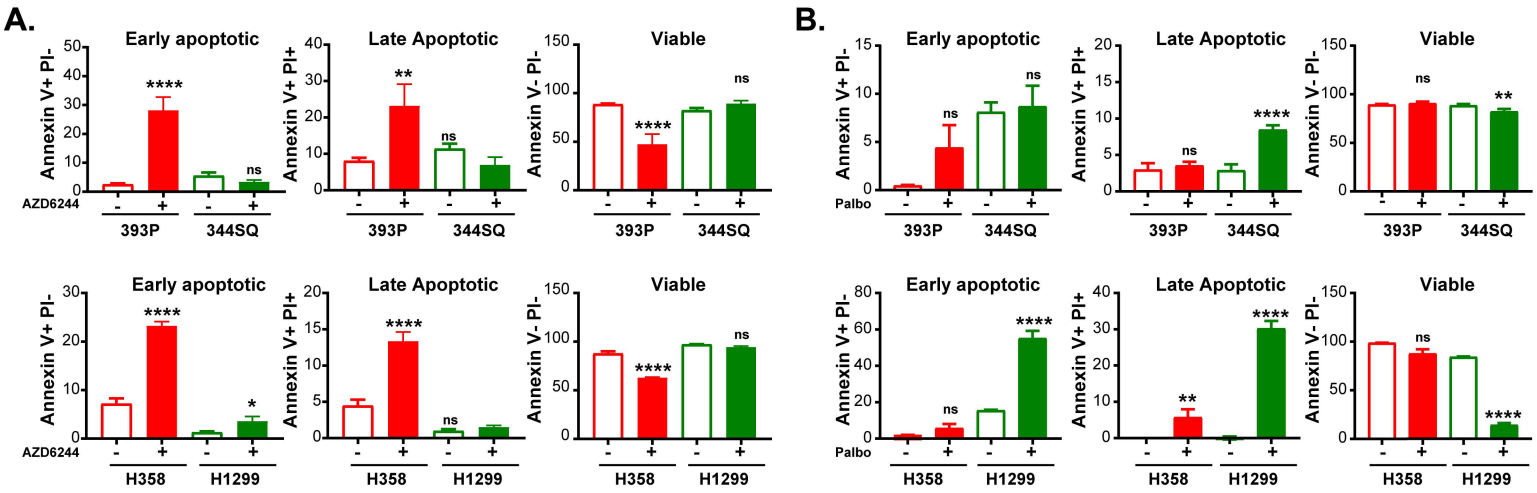

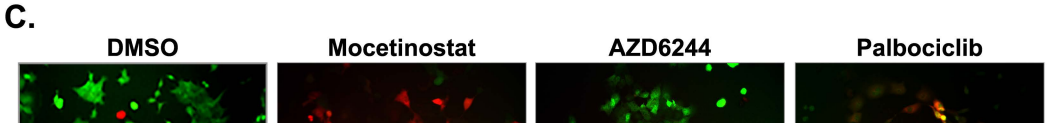

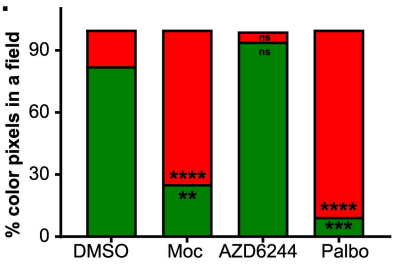

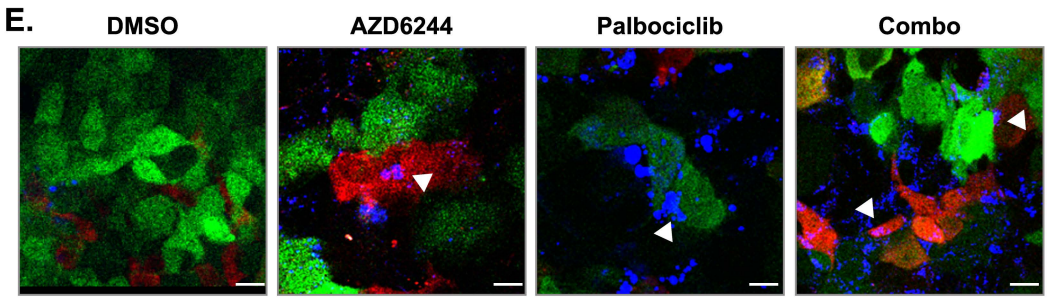

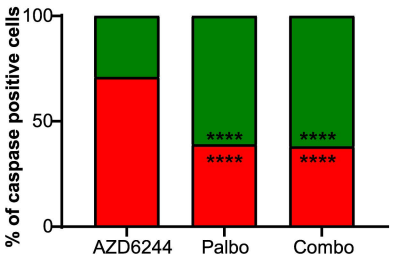

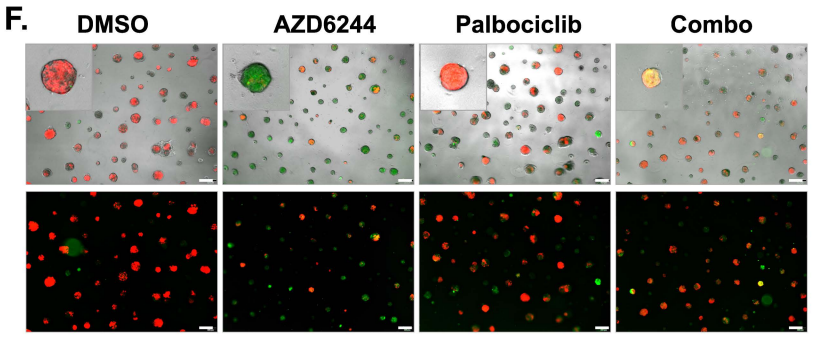

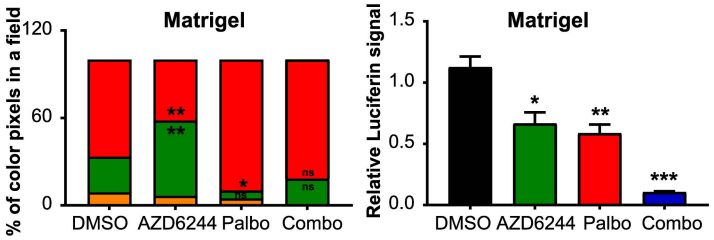

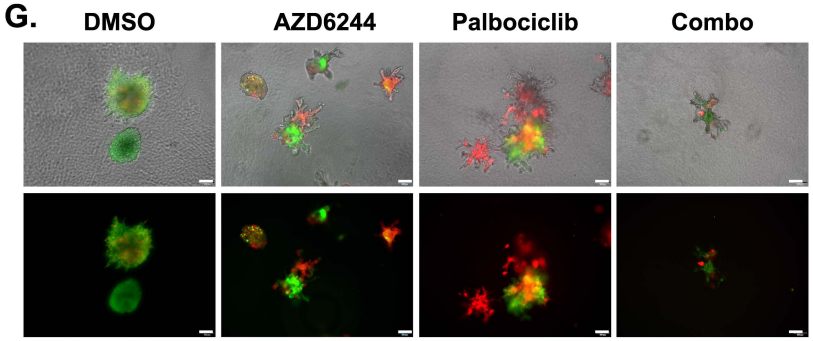

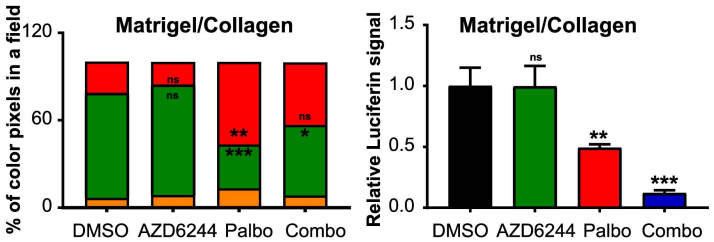

Fig. 6: Combination of CDK4 and MEK inhibitors controls syngeneic tumor growth and prevents emergence of EMT-mediated resistance

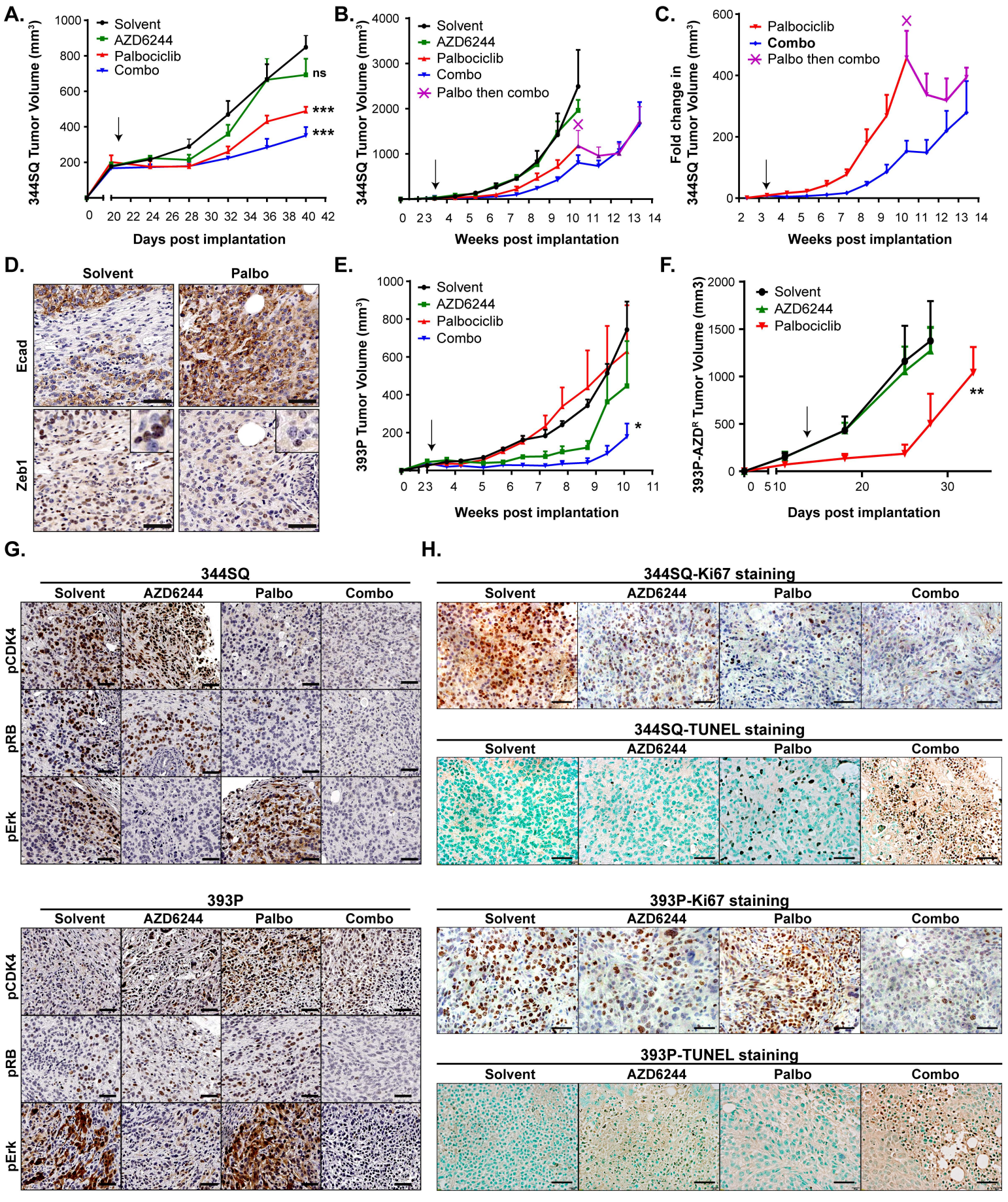

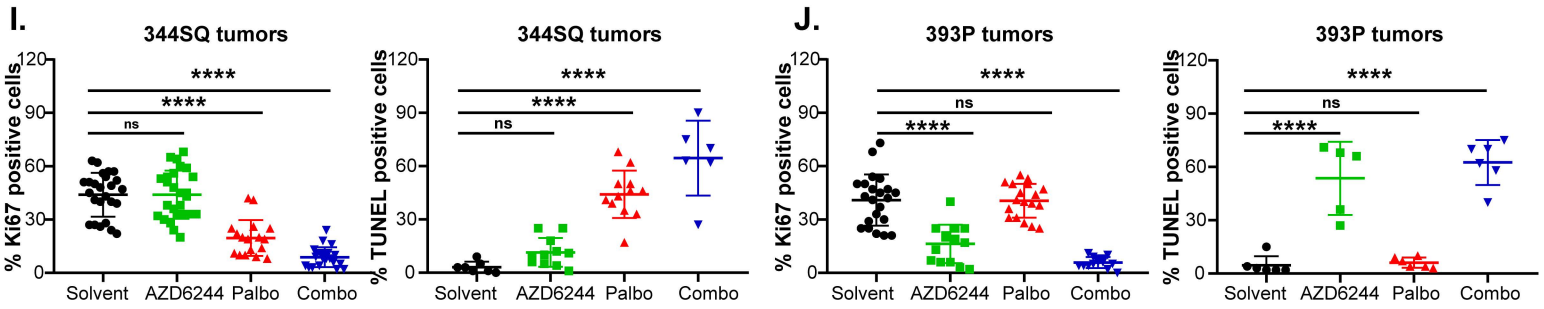
I.
344SQ tumors
% Ki67 positive cells
120
90
60
30
0
****
****
ns
Solvent
AZD6244
Palbo
Combo
344SQ tumors
% TUNEL positive cells
120
90
60
30
0
****
****
ns
Solvent
AZD6244
Palbo
Combo
J.
393P tumors
% Ki67 positive cells
120
90
60
30
0
****
ns
****
Solvent
AZD6244
Palbo
Combo
393P tumors
% TUNEL positive cells
120
90
60
30
0
****
ns
****
Solvent
AZD6244
Palbo
Combo

Fig. 7: Concomitant targeting of CDK4 and MAPK pathways augments response in Kras mutant autochthonous lung tumors

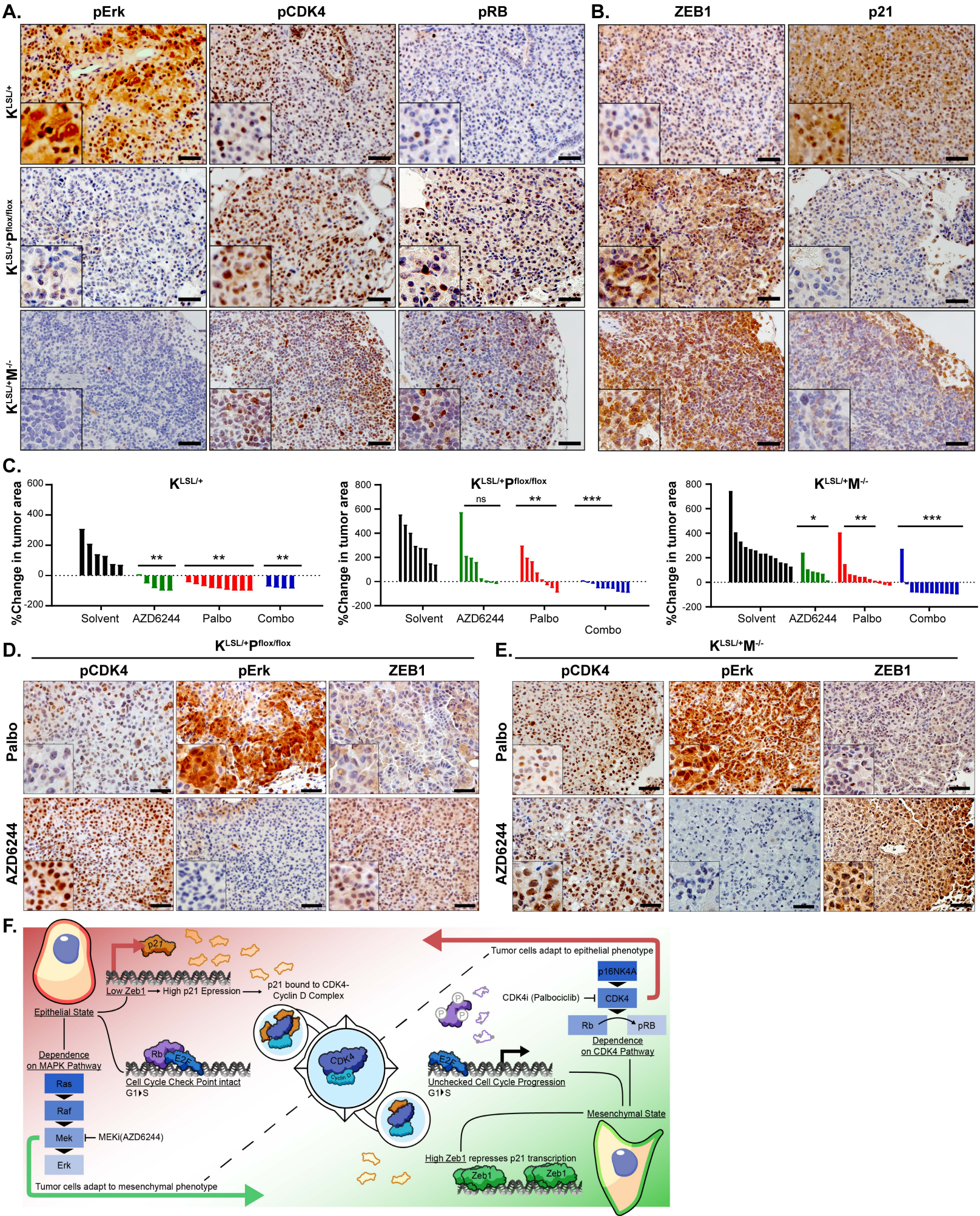

Figures

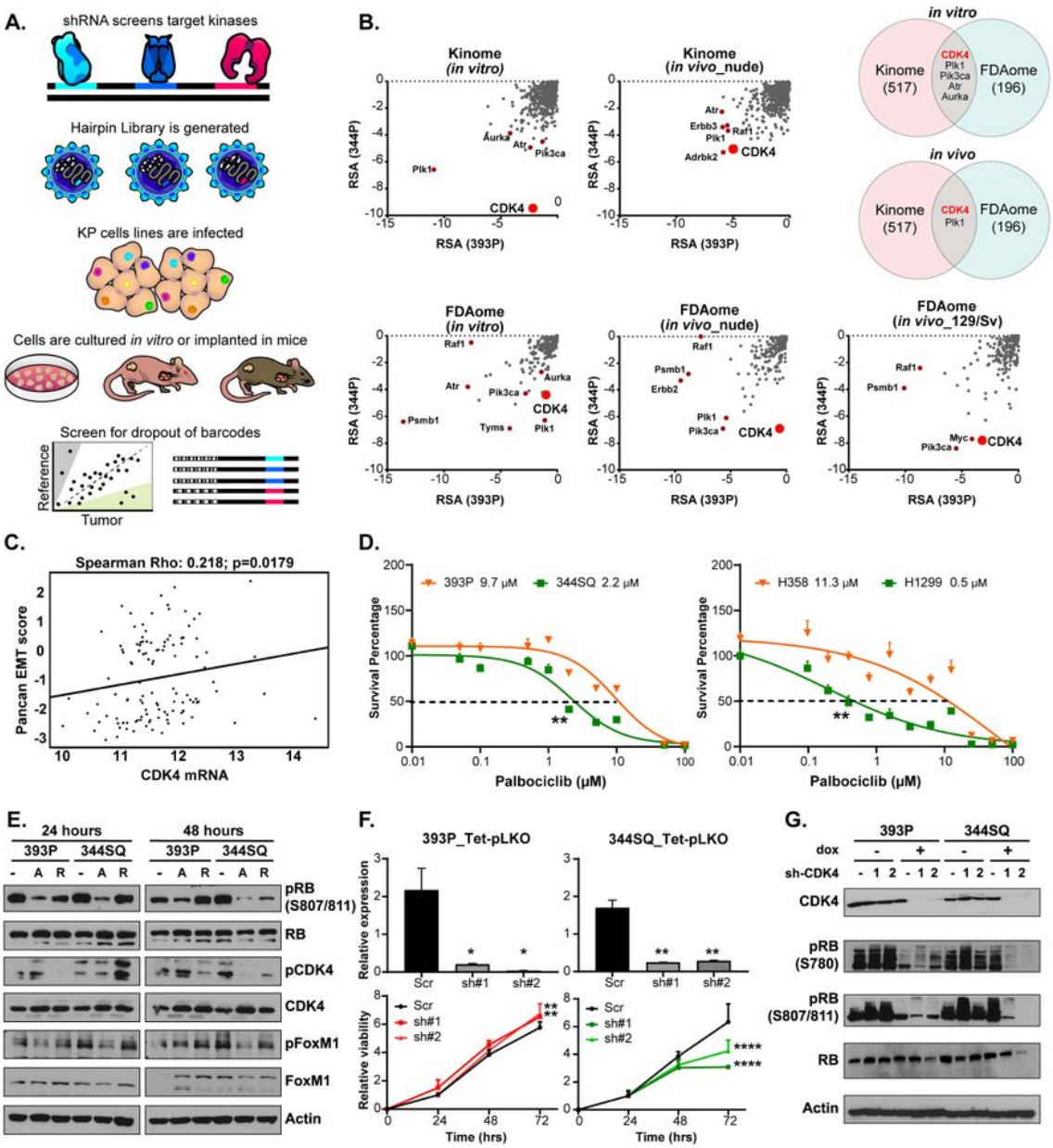

Figure 1

Mesenchymal lung cancer cells exhibit increased dependency on CDK4 for growth. (A) Schematic illustration of the workflow of the shRNA dropout screens. A library of lentiviral particles expressing 10 different barcoded shRNAs was transduced into murine KP mutant lung cancer cells. The cells were

cultured in vitro or implanted in nude or syngeneic 129/Sv mice and later sequenced for barcoded shRNAs and compared to reference cells. (B) Results from Kinome and FDAome shRNA dropout screens in 393P (epithelial) and 344P (mesenchymal) cell lines and tumors compared based on the redundant shRNA activity (RSA). Top differential hits are labeled on the graphs, most important being CDK4 (red). Venn diagram shows comparisons across different conditions and top hits identified. (C) Cluster plot analysis of Spearman's rank correlation between EMT score and CDK4 mRNA expression of 118 human NSCLC cell lines. (D) In vitro cell viability after 48 hour palbociclib treatment in a panel of epithelial and mesenchymal murine (393P, 344SQ) and human (H358, H1299) lung cancer cell lines. n=8 per drug concentration. The curve was generated using a nonlinear regression fit model. (E) Western blot showing the effect on signaling in 393P and 344SQ tumor cells upon treatment with abemaciclib (A: 2 μM) and ribociclib (R: 2 μM) for 24 and 48 hours. (F) Top: Relative mRNA expression of CDK4 upon doxycycline mediated induction of shRNAs targeting CDK4 at 72 hours. Bottom: Growth rates of 393P and 344SQ cells with or without CDK4 knockdown over 72 hours measured by MTT assay. One and two-way ANOVA test was used for statistical analysis, respectively. (G) Western blot analysis of CDK4 pathway after 72 hours of CDK4 knockdown. **** $p<0.0001$; ** $p<0.001$.

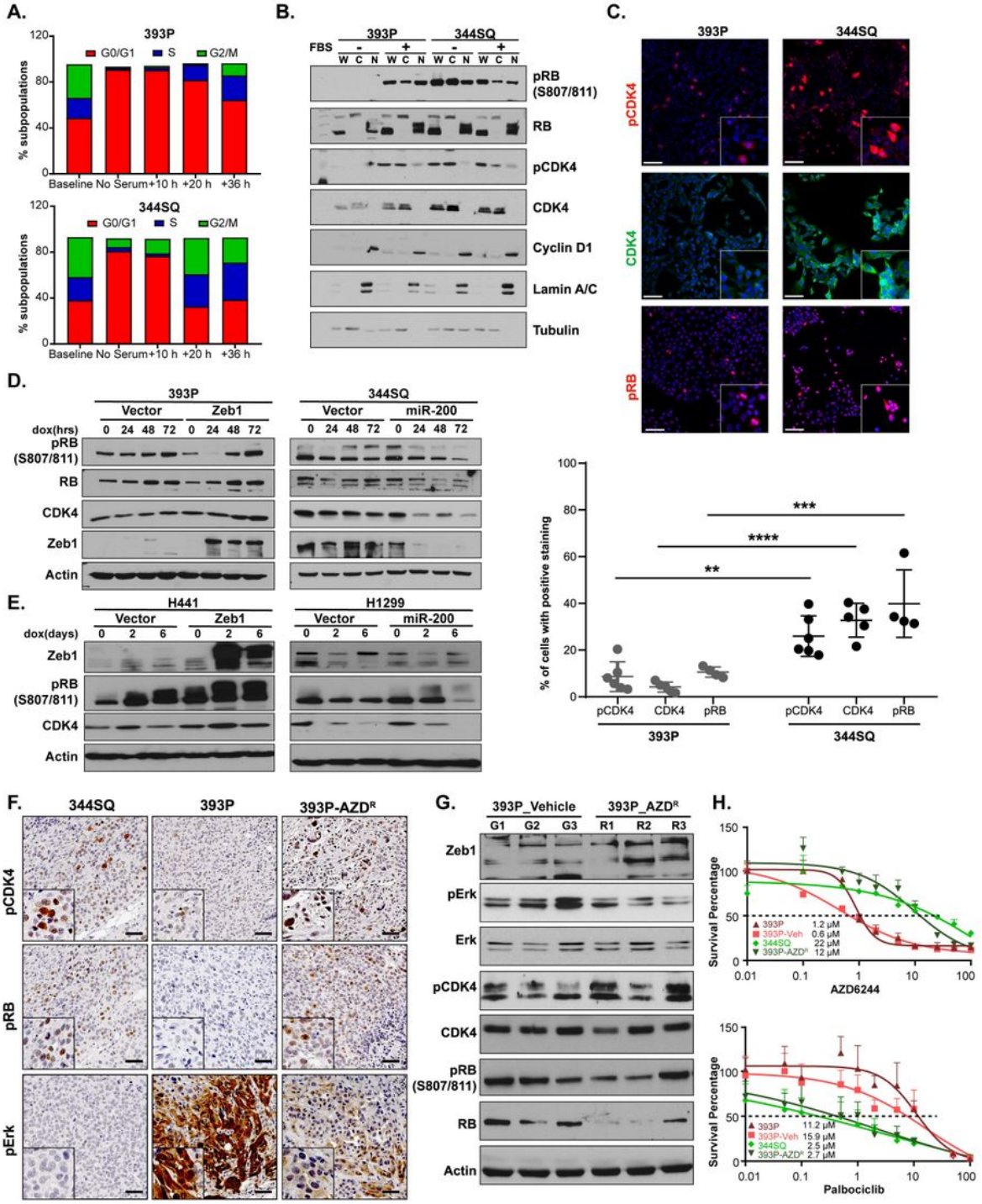

Figure 2

The CDK4 pathway is dynamically regulated by the EMT 740 status of tumor cells (A) Cell cycle analysis 393P and 344SQ cells using propidium iodide (PI). Baseline cell cycle was determined by staining cells in culture with PI. Cell cycle arrest was induced by serum starvation of cells for 24 hours followed by release into cell cycle by addition of FBS containing media and analyzed after 10, 20 and 36 hours. (B) Subcellular fractionation followed by western blot analysis of indicated cell cycle markers. (C) Top:

Representative images of immunofluorescence on 393P and 344SQ wild type cells for indicated markers. Scale bar: 50 μM. Bottom: 4-6 biological replicates were analyzed for quantification of the fluorescent signal. One-way ANOVA was used for statistical analysis. (D-E) Western blot analysis of murine (D) and human (E) cells with ZEB1 and miR-200 expression. Cells were induced with 2 μg/ml of doxycycline for times indicated. (F) Immunohistochemistry on tumors derived from 393P, 344SQ and 393P_AZDR tumors for indicated markers. Scale bar: 50 μM (G) Western blot analysis on cell lines derived from 393P tumors treated with vehicle or AZD6244 for indicated markers. (H) In vitro cell viability assay on 393P, 344SQ, 393P_vehicle and 393P_AZDR after 48 hours of AZD6244 and palbociclib treatment. n=8 per drug concentration. The curve was generated using a nonlinear regression fit model. **** p<0.0001; *** p<0.005; ** p<0.001.

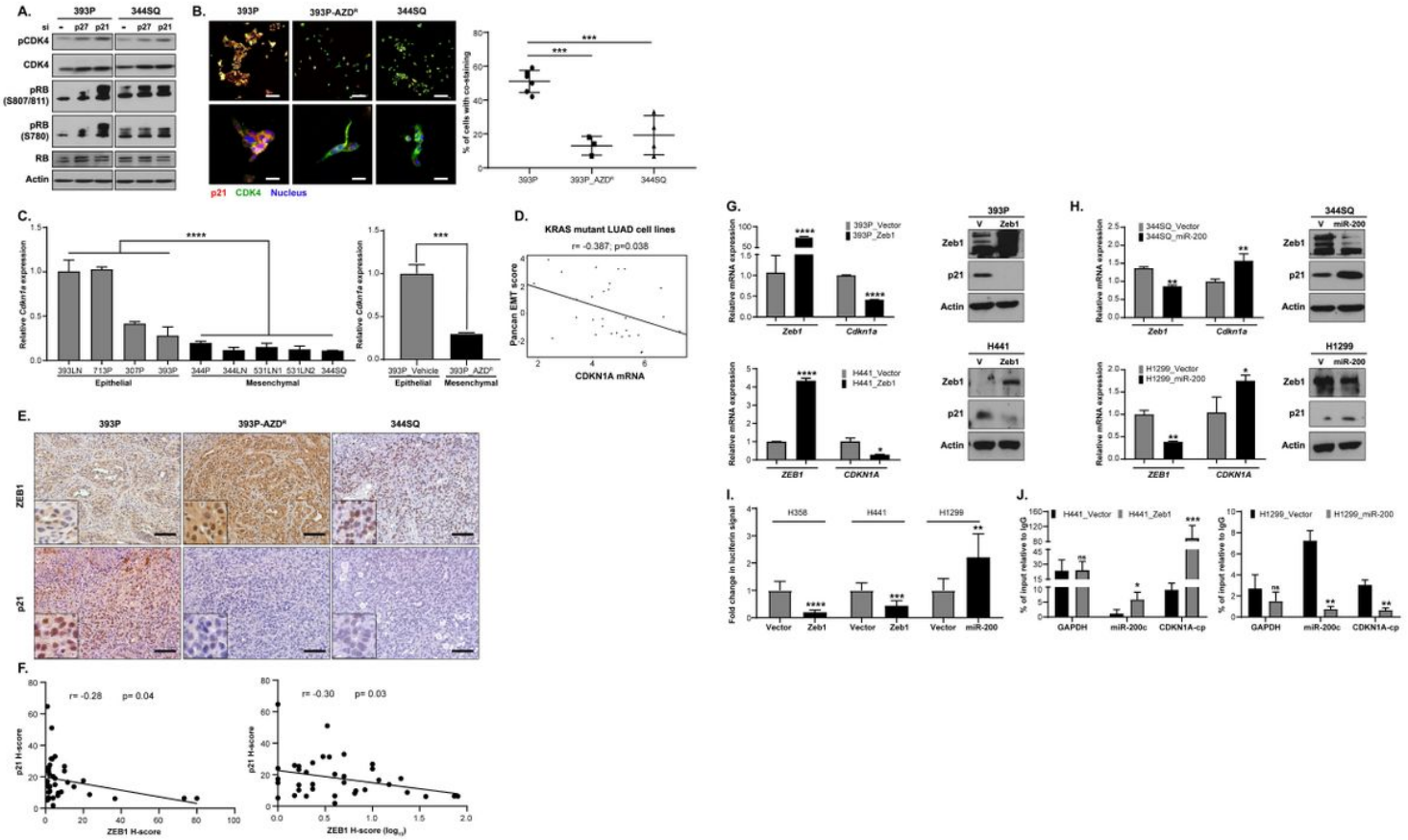

Figure 3

ZEB1 regulates p21 expression and causes differential 756 CDK4 pathway activation. (A) Transient knockdown of p21 and p27 using 20 nM si-RNAs for 48 hours in 393P and 344SQ cells followed by western blot analysis. (B) (Left) Immunofluroscent staining of 393P, 393P_AZDR and 344SQ cells. Scale bar top: 100 μM, bottom: 10 μM. (Right) Quantification of cells co-staining positive for CDK4 and p21 in each cell lines. 4-6 biological replicates were analyzed for quantification of the fluorescent signal. (C) Relative expression of Cdkn1a mRNA in a panel of epithelial and mesenchymal murine lung cancer cells (left) and 393P vehicle and AZDR cell lines (right). (D) Cluster plot analysis of Pearson's correlation between CDKN1A mRNA and EMT score in 29 KRAS mutant human lung adenocarcinoma cell lines. (E)

Immunohistochemistry on tumors derived from 393P, 344SQ and 393P-AZDR cells Scale bar: 50 μM. (F) Cluster plot analysis of Pearson's correlation between ZEB1 and p21 H scores in NSCLC specimens. (G and H) Relative expression of Cdkn1a mRNA and p21 protein levels upon induction of EMT or MET. ZEB1 induction for 48 hours with 2 μg/ml of doxycycline in murine (G, top) and human (G, bottom) epithelial lung cancer cell lines. miR-200 induction for 48 hours with 2 μg/ml of doxycycline in murine (H, top) and human (H, bottom) mesenchymal lung cancer cell lines. (I) Luciferase reporter assay to determine relative luciferase activity of CDKN1A promoter reporter construct transfected into epithelial H358 and H441 cells with induced ZEB1 expression or mesenchymal H1299 with induced miR-200 expression. Relative luciferin signal was normalized to promoter-less vector control signal. (J) Fold enrichment by qPCR analysis of CDKN1A promoter containing ZEB1 binding site after endogenous ZEB1 ChIP in H441 cells with inducible ZEB1 expression or H1299 cells with inducible miR-200 expression, using ZEB1 antibody or immunoglobulin G (IgG) control antibody. One-way ANOVA was used for statistical analysis in all the panels. **** $p<0.0001$; *** $p<0.005$; ** $p<0.001$; * $p< 0.05$; ns: not significant.

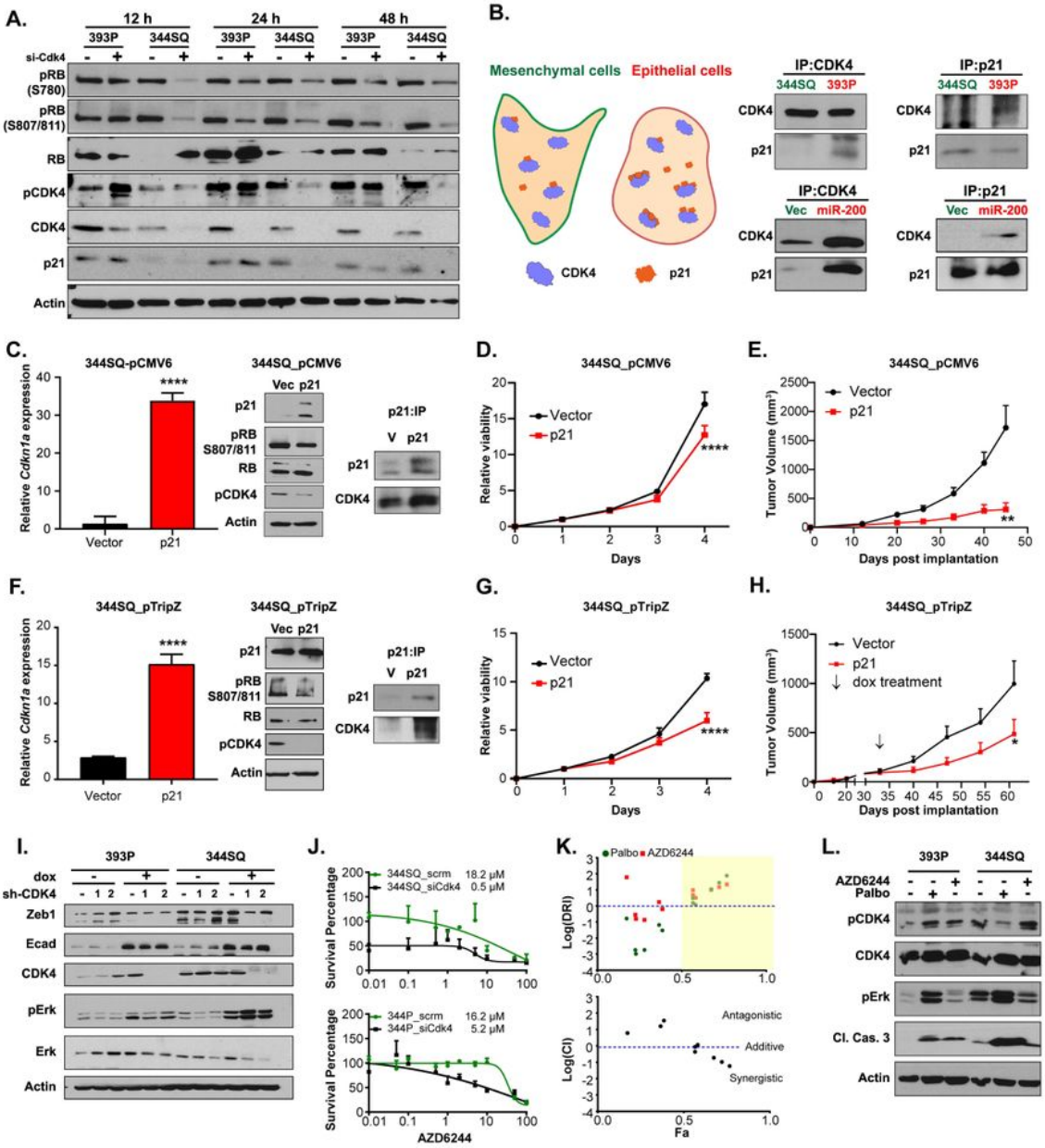

Figure 4

Suppression of p21 in mesenchymal cells regulates 779 CDK4 pathway. (A) Transient knockdown of CDK4 using 20 nM si-RNAs for 12, 24 and 48 hours in epithelial and mesenchymal cancer cells followed by western blot analysis. (B) (Left) Graphical representation of the differences in CDK4-p21 complex formation in epithelial and mesenchymal cancer cells. (Right) Co-IP of endogenous CDK4 and p21 in epithelial (393P and 344SQ_miR-200) and mesenchymal (344SQ and 344SQ_vec) cell lines and analyzed

by western blot with anti-CDK4 and anti-p21 antibodies. (C) Constitutive overexpression of Cdkn1a in 344SQ cell lines. Relative mRNA expression of Cdkn1a (left), western blot analysis of CDK4 pathway (middle) and co-IP of CDK4 and p21 in 344SQ cells (right). (D) Growth rates of 344SQ cells ± p21 constitutive overexpression over 4 days measured by WST-1 assay. (E) Tumor volume measurements at indicated time points of 344SQ tumors + p21 (n= 5 per group). Data are presented as mean ± SEM. (F) Doxycycline induced overexpression of Cdkn1a in 344SQ cell lines for 48 hours. Relative mRNA expression of Cdkn1a (left), western blot analysis of CDK4 pathway (middle) and co-IP of CDK4 and p21 in 344SQ cells (right). (G) Growth rates of 344SQ cells ± p21 overexpression (doxycycline induced) over 4 days measured by WST-1 assay. (H) Tumor volume measurements at indicated time points of 344SQ tumors + p21 expression with doxycycline feed (n=9-10/group). Dox feed was started after tumors reached a size of 100-150 mm3 (indicated by arrow). Data are presented as mean ± SEM. (I) Western blot of EMT markers with CDK4 knockdown for 72 hours. (J) In vitro cell viability assay on 344SQ (top) and 344P (bottom) lung cancer cell lines with or without transient knockdown of CDK4 and treatment with a range of concentrations of AZD6244 for 48 hours. n=8 per drug concentration. The curve was generated using a nonlinear regression fit model. (K) Palbociclib and AZD6244 were used to determine the Drug Reduction Index (DRI) and Combination Index (CI) using Chou-Talalay method on 344SQ cells. (L) Western blot analysis on cells treated with AZD6244 (5μM) and palbociclib (5μM) for 48 hours. Cleaved caspase-3 was used as an apoptotic marker. Statistical analysis for C, E, F and H: Unpaired t-test and for D and G: Two-way ANOVA test. **** $p<0.0001$; *** $p<0.005$; ** $p<0.001$; * $p< 0.05$.

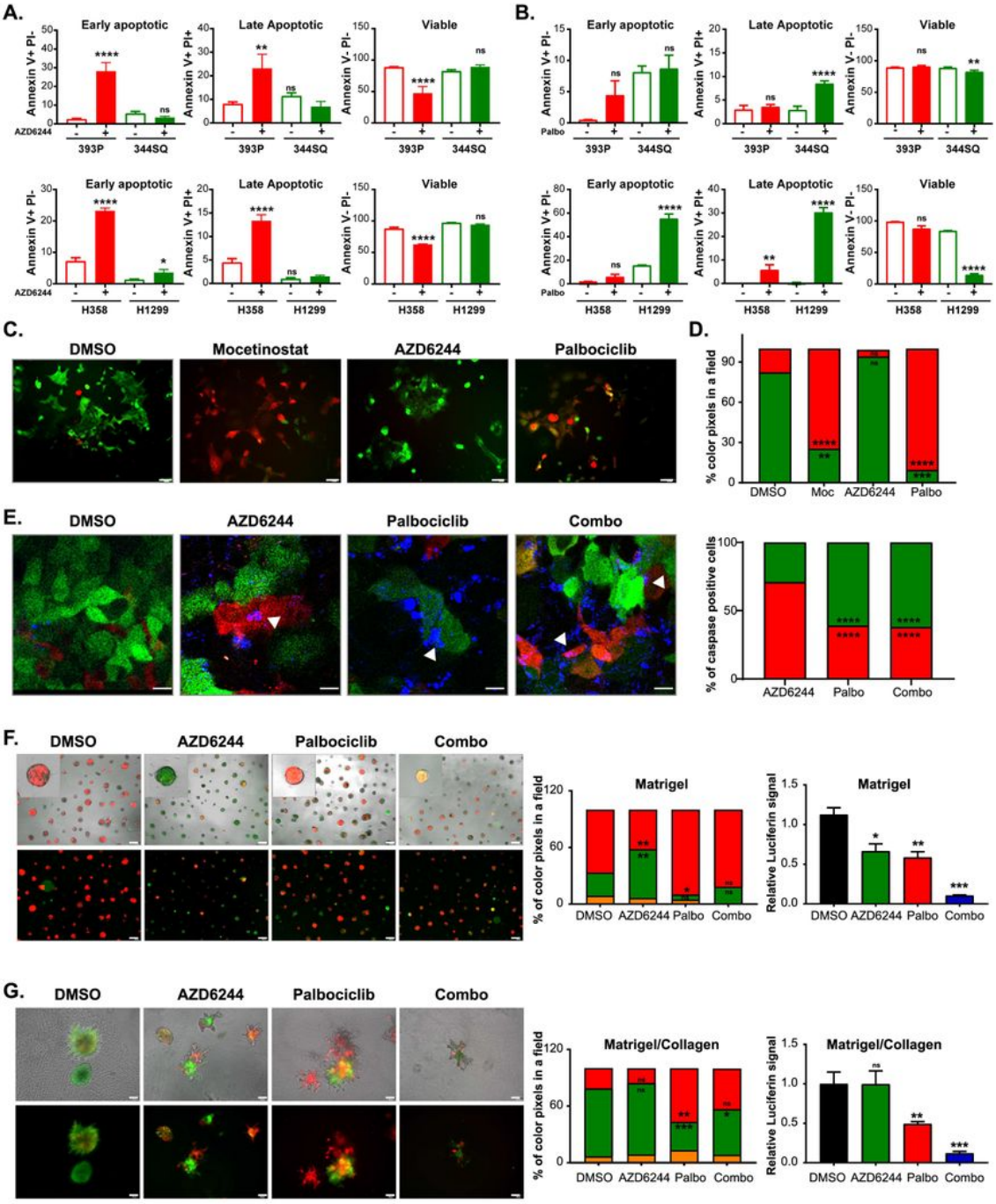

Figure 5

Co-targeting CDK4 and MAPK pathways targets d 805 ifferent tumor cell subsets. (A-B) Apoptosis was determined by annexin V and propidium iodide staining of murine and human lung cancer cells after treatment with AZD6244 (5 μM) or palbociclib (5 μM) for 48 hours. The data are presented as the mean ± SD from three replicates. (C) 344SQ_Z-cad cells were treated with DMSO, mocetinostat (1 μM), AZD6244 (5 μM), or palbociclib (5 μM) for 48 hours followed by fluorescent image acquisition. Scale bar: 50 μM.

(D) Images from (C) were quantified for the percentage of RFP or GFP color pixels calculated per field of view (FOV). n=4-6 FOVs. (E) 344SQ_Z-cad cells were treated with DMSO, AZD6244 (5 μM), palbociclib (5 μM) or the combination. NucView® 405 Caspase 3 substrate was added to each condition as a readout for apoptosis. Representative fluorescent images were acquired 48 hours after addition of drugs (left). Scale bar = 25 μM. Arrows indicate apoptotic cells. Images were quantified for total caspase- 3+ cells as a percentage of total cells in 4-6 FOVs (right). (F-G) Ex vivo tumors (EVTs) were plated in a Matrigel (MG) or a Collagen/Matrigel (Coll/MG) matrix. After 24 hours, EVTs were treated with DMSO, AZD6244 (5 μM), palbociclib (5 μM) or the combination. (F) Treatment in MG was continued for 9 days with representative images from last day of the culture shown (left panel, scale bar: 200 μM). Percentage of RFP and GFP color pixels in 4-6 FOVs (middle panel). Data are represented as mean. At the end of the treatment, Cell Titer-Glo reagent was added and relative luciferin signal was measured (right panel). (G) EVTs in Coll/MG matrix were treated for 5 days. Representative images at the end of experiment shown (left panel, scale bar: 100 μM), quantification of percentage RFP and GFP color pixels in 4-6 FOVs (middle panel) and relative luciferin signal using Cell Titer-Glo reagent (right panel). Treatment groups were compared to DMSO using one-way ANOVA in all the panels. **** p<0.0001; *** p<0.005; ** p<0.001; * p< 0.05; ns: not significant.

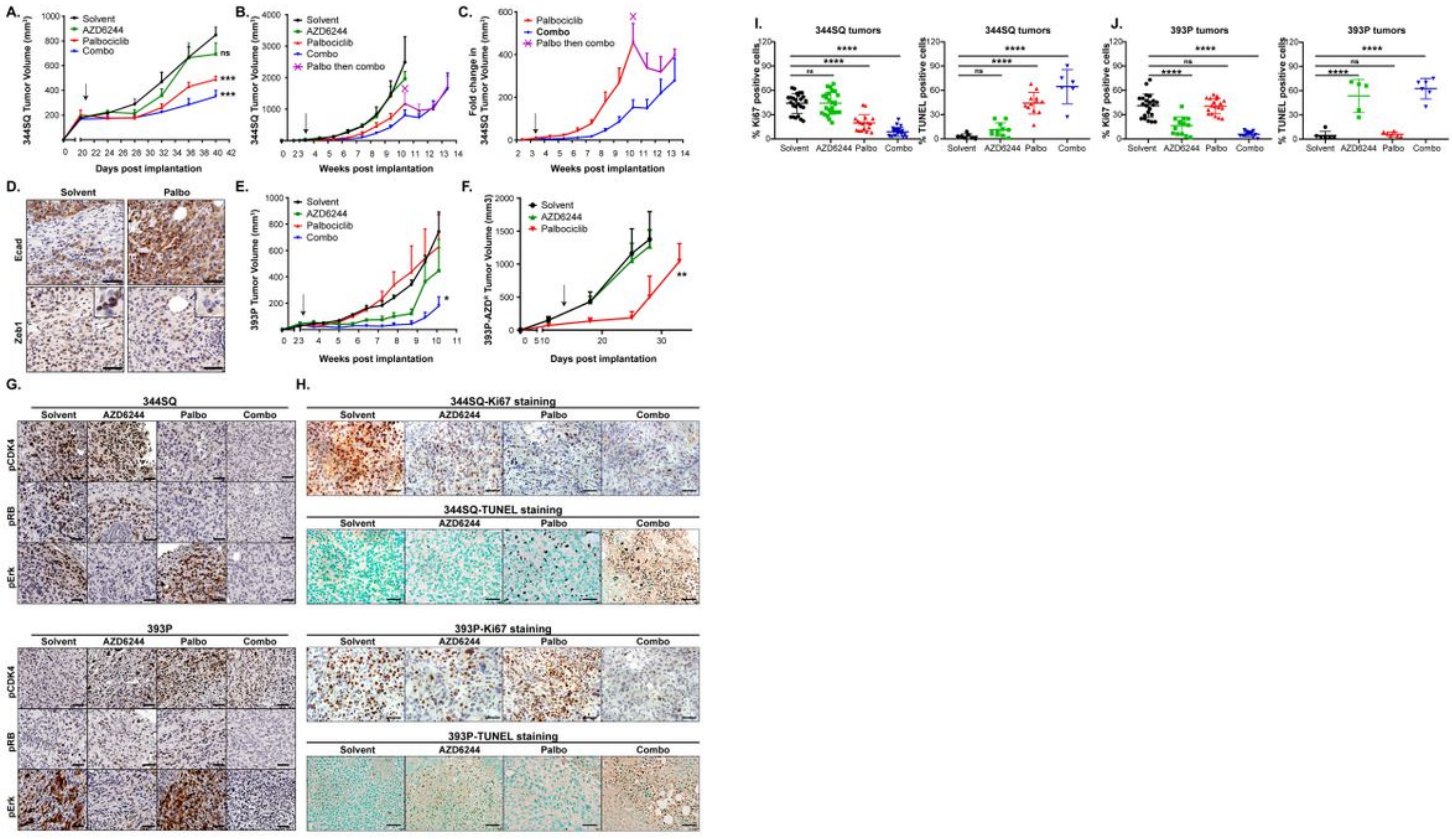

Figure 6

Combination of MEK and CDK4 inhibitors cont 828 rols syngeneic tumor growth and prevents emergence of EMT mediated resistance. (A) In vivo volume measurements at the indicated time points for 344SQ subcutaneous tumors in syngeneic WT mice (n=5 per group) after daily treatment with solvent, AZD6244

(25 mg/kg), palbociclib (50 mg/kg) or combination. Arrow indicates start of the treatment. (B) 344SQ subcutaneous tumors were treated with solvent (n=5), AZD6244 (25 mg/kg) (n=10), palbociclib (50 mg/kg) (n=10) or combination (n=5) for 7 weeks at which point resistance to palbociclib emerged. 5 mice from palbociclib treatment alone arm were converted to combination arm and treatment was continued for another 3 weeks (marked by purple X). (C) Fold change in 344SQ tumors in the palbociclib and combo arms over 13 weeks. (D) Immunohistochemical analysis on 344SQ tumors treated with solvent or palbociclib for 7 weeks with indicated markers. Scale bar: 50 μM. (E) In vivo volume measurements at indicated time points for 393P subcutaneous tumors in syngeneic WT mice (n=5 per group) after daily treatment with solvent, AZD6244 (25 mg/kg), palbociclib (50 mg/kg) or combination. Arrow indicates start of treatment. (F) In vivo volume measurements of 393P-AZDR subcutaneous tumors in syngeneic WT mice (n=5 per group) after daily treatment with AZD6244 (25 mg/kg) or palbociclib (50 mg/kg). Arrow indicates start of treatment at day 14. (G) IHC analysis on 344SQ and 393P tumors harvested from (A) and (E) respectively, with indicated markers. Scale bar: 50 μM. (H-J) Tumors from the experiments described in (A) and (E) were stained with Ki67 and TUNEL assay to measure cell proliferation and cell death respectively. Representative IHC images are shown in (H). Scale bar: 50 μM. Images were quantified for Ki67 (I) and TUNEL (J) staining in each treatment group. n=2-3 per group with 3-6 FOV per mouse. Statistical significance was determined by one-way ANOVA in all the panels. **** $p<0.0001$; *** $p<0.005$; ** $p<0.001$; * $p< 0.05$; ns: not significant.

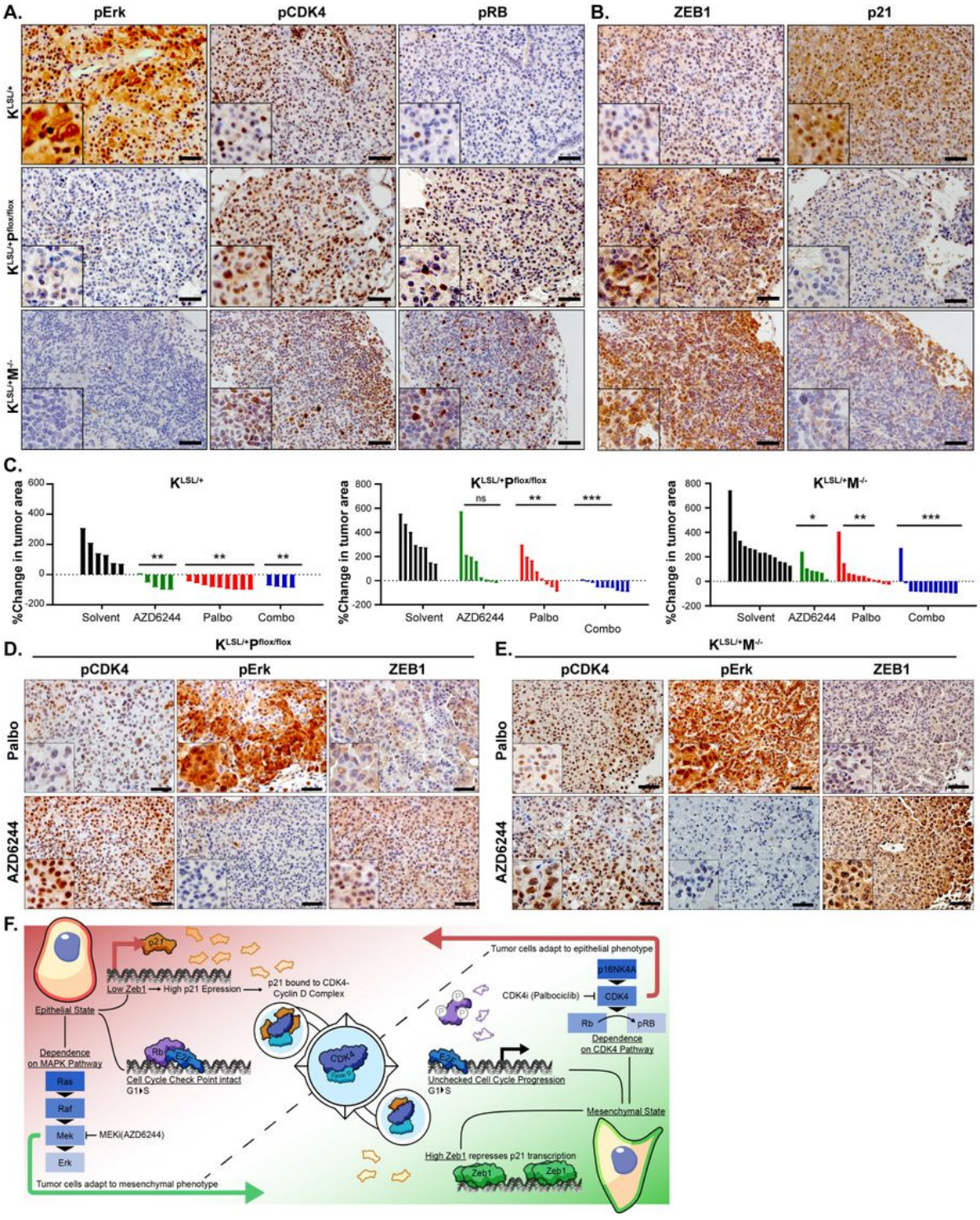

Figure 7

Concomitant targeting of CDK4 and MAPK 851 pathways augments response in Kras mutant autochthonous lung tumors. (A) Immunohistochemistry for indicated markers on KrasLSL/+, Kras LSL/+Pflox/flox and Kras LSL/+M-/- lung sections 18-20 weeks post Ad-Cre infection. Scale bar: 50 μM. (B) Immunohistochemistry for indicated markers on KrasLSL/+, Kras LSL/+Pflox/flox and Kras LSL/+M-/- lung sections 18-20 weeks post Ad-Cre infection. Scale bar: 50 μM. (C) Percentage change in

overall lung tumor area of KrasLSL/+, Kras LSL/+Pflox/flox and Kras LSL/+M-/- mice after 6-8 weeks of daily treatment with AZD6244 (25 mg/kg), palbociclib (50 mg/kg) or both as assessed by micro-CT imaging of mouse lungs. Significance was determined using Brown-Forsythe and Welch ANOVA tests. (D and E) Immunohistochemistry for indicated markers on lung sections from mice treated Kras LSL/+Pflox/flox (D) and Kras LSL/+M-/- (E) treated with AZD6244 and palbociclib for 6-8 weeks. Scale bar: 50 μM. (F) Proposed working model demonstrating differential CDK4 and MAPK signaling pathway activation and sensitivity to CDK4 and MEK inhibitor treatments between epithelial and mesenchymal lung cancer cells due to ZEB1 regulation of p21 expression.

Supplementary Files

This is a list of supplementary files associated with this preprint. Click to download.

- CDK4Supplementaryfiles.pdf